

Improving Robust Generalization by Direct PAC-Bayesian Bound Minimization

Zifan Wang^{1*} Nan Ding^{2†} Tomer Levinboim² Xi Chen² Radu Soricut²
Carnegie Mellon University¹ Google Research²

zifan@cmu.edu, {dingnan, tomerl, chillxichen, rsoricut}@google.com

Abstract

Recent research in robust optimization has shown an overfitting-like phenomenon in which models trained against adversarial attacks exhibit higher robustness on the training set compared to the test set. Although previous work provided theoretical explanations for this phenomenon using a robust PAC-Bayesian bound over the adversarial test error, related algorithmic derivations are at best only loosely connected to this bound, which implies that there is still a gap between their empirical success and our understanding of adversarial robustness theory. To close this gap, in this paper we consider a different form of the robust PAC-Bayesian bound and directly minimize it with respect to the model posterior. The derivation of the optimal solution connects PAC-Bayesian learning to the geometry of the robust loss surface through a Trace of Hessian (TrH) regularizer that measures the surface flatness. In practice, we restrict the TrH regularizer to the top layer only, which results in an analytical solution to the bound whose computational cost does not depend on the network depth. Finally, we evaluate our TrH regularization approach over CIFAR-10/100 and ImageNet using Vision Transformers (ViT) and compare against baseline adversarial robustness algorithms. Experimental results show that TrH regularization leads to improved ViT robustness that either matches or surpasses previous state-of-the-art approaches while at the same time requires less memory and computational cost.

1. Introduction

Despite their success in a wide range of fields and tasks, deep learning models still remain susceptible to manipulating their outputs by even tiny perturbations to the input [6, 7, 10, 20, 31, 33, 44, 48].

Several lines of work have focused on developing robust

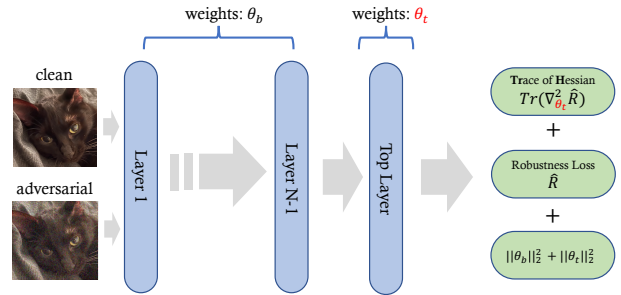


Figure 1. We propose Trace of Hessian (TrH) regularization for training adversarially robust models. In addition to an ordinary robust loss (e.g., TRADES [55]), we regularize the TrH of the loss with respect to the weights of the top layer to encourage flatness. The training objective is the result of direct PAC-Bayesian bound minimization in Theorem 3.

training techniques against such adversarial attacks [8, 21, 32, 33, 37, 42, 47, 49, 55]. Importantly, Rice et al. [39] observe a robust overfitting phenomenon, referred to as the *robust generalization gap*, in which a robustly-trained classifier shows much higher accuracy on adversarial examples from the training set, compared to lower accuracy on the test set. Indeed, several technical approaches have been developed that could alleviate this overfitting phenomenon, including ℓ_2 weight regularization, early stopping [39], label smoothing, data augmentation [52, 54], using synthetic data [22] and etc.

According to learning theory, the phenomenon of overfitting can be characterized by a PAC-Bayesian bound [4, 9, 19, 35, 43] which upper-bounds the expected performance of a random classifier over the underlying data distribution by its performance on a finite set of training points plus some additional terms.

Although several prior works [22, 25, 27, 50] have built upon insights from the PAC-Bayesian bound, none attempted to directly minimize the upper bound, likely due to the fact that the minimization of their forms of the PAC-

*Work done during internship in Google.

†Corresponding author

Bayesian bound do not have an analytical solution.

In this paper, we rely on a different form of the PAC-Bayesian bound [19], which can be readily optimized using a Gibbs distribution [17] with which we derive a second-order upper bound over the robust test loss. Interestingly, the resulting bound consists of a regularization term that involves *Trace of Hessian* (TrH) [13] of the network weights, a well-known measure of the loss-surface flatness.

For practical reasons, we limit TrH regularization to the top layer of the network only because computing a Hessian matrix and its trace for the entire network is too costly. We further derive the analytical expression of the top-layer TrH and show both theoretically and empirically that top-layer TrH regularization has a similar effect as regularizing the entire network. The resulting TrH regularization (illustrated in Figure 1) is less expensive and more memory efficient compared to other competitive methods [22, 25, 27, 50].

In summary, our contributions are as follows: (1) We provide a PAC-Bayesian upper-bound over the robust test loss and show how to directly minimize it (Theorem 3). To the best of our knowledge, this has not been done by prior work. Our bound includes a TrH term which encourages the model parameters to converge at a flat area of the loss function; (2) Taking efficiency into consideration, we restrict the TrH regularization to the top layer only (Algorithm 1) and show that it is an implicit but empirically effective regularization on the TrH of each internal layer (Theorem 4 and Example 1); and (3) Finally, we conduct experiments with our new TrH regularization and compare the results to several baselines using Vision Transformers [15]. On CIFAR-10/100, our method consistently matches or beats the best baseline. On ImageNet, we report a significant gain (+2.7%) in robust accuracy compared to the best baseline and establish a new state-of-the-art result of 48.9%.

2. Background

We begin by introducing our notation and basic definitions. Let $g_\theta(x)$ denote the output logits of a network θ on an input $x \in \mathcal{X}$. We denote the predicted label by $F_\theta(x) = \arg \max g_\theta(x) \in \mathcal{Y}$ and the softmax output of g_θ by $s(g_\theta)$. To train the network, we sample a dataset $D^m \stackrel{\text{def}}{=} \{(x_i, y_i)\}_{i=0}^{m-1}$ containing m i.i.d examples from a distribution \mathcal{D} , so that the test and training losses are

$$L(\theta, \mathcal{D}) \stackrel{\text{def}}{=} \mathbb{E}_{(x,y) \sim \mathcal{D}} l((x, y), g_\theta),$$

$$\text{and } \hat{L}(\theta, D^m) \stackrel{\text{def}}{=} \frac{1}{m} \sum_{(x,y) \in D^m} l((x, y), g_\theta),$$

respectively and l denotes the loss function. Ideally, the classification error of g_θ should be represented by the 0-1 loss $l((x, y), g_\theta) = \mathbb{I}[F_\theta(x) \neq y]$. However, since the 0-1 loss is infeasible to minimize and inferior for generalization, it is common to use surrogate losses such as the

Cross-Entropy loss $\text{CE}((x, y), g_\theta) = -\log\{s(g_\theta(x))\}_y$ for training instead, where $\{v\}_j$ denotes the j -th element of the vector v . Finally, we denote the KL-divergence between two distributions \mathcal{P}, \mathcal{Q} as $\text{KL}(\mathcal{P}||\mathcal{Q})$. For any twice-differentiable function L , we denote its Jacobian and Hessian matrix as ∇L and $\nabla^2 L$ respectively.

2.1. Adversarial Robustness

The goal of *adversarial robustness* is to train a deep network that is robust against ℓ_p norm-bounded noises. In this case, the test and training loss functions are replaced by their respective robust counterparts $R(\theta, \mathcal{D})$ on the test set and $\hat{R}(\theta, D^m)$ on the training set, such that

$$R(\theta, \mathcal{D}) \stackrel{\text{def}}{=} \mathbb{E}_{(x,y) \sim \mathcal{D}} \max_{\|\epsilon\|_p \leq \delta} l((x + \epsilon, y), g_\theta),$$

$$\text{and } \hat{R}(\theta, D^m) \stackrel{\text{def}}{=} \frac{1}{m} \sum_{(x,y) \in D^m} \max_{\|\epsilon\|_p \leq \delta} l((x + \epsilon, y), g_\theta),$$

where δ is the maximum noise budget. Various methods have been proposed to improve adversarial robustness. In this paper, we focus on the following two well-known defenses: *adversarial training* [33], denote AT (Definition 1), and TRADES [55] (Definition 2). AT is a classical method in enforcing robustness; while TRADES achieves state-of-the-art robust accuracy on CIFAR-10 and ImageNet [22].

Definition 1 (Adversarial Training (AT) [33]) *Given a network with parameter θ , a training set D^m , the bound of noise δ and norm $\|\cdot\|_p$, AT minimizes the following objective w.r.t θ ,*

$$\hat{R}_{AT}(\theta, D^m) \stackrel{\text{def}}{=} \frac{1}{m} \sum_{(x,y) \in D^m} \max_{\|\epsilon\|_p \leq \delta} \text{CE}((x + \epsilon, y), g_\theta).$$

which considers the adversarial sample $x + \epsilon$ in a δ -ball around each input, instead of the input itself.

Definition 2 (TRADES [55]) *Given the same assumptions as in Definition 1, TRADES minimizes the following objective w.r.t θ :*

$$\hat{R}_T(\theta, D^m) \stackrel{\text{def}}{=} \frac{1}{m} \sum_{(x,y) \in D^m} \left[\text{CE}((x, y), g_\theta) + \lambda_t \cdot \max_{\|\epsilon\|_p \leq \delta} \text{KLoss}((x, x + \epsilon), g_\theta) \right]$$

where $\text{KLoss}((x, x + \epsilon), g_\theta) = \text{KL}(s(g_\theta(x))||s(g_\theta(x + \epsilon)))$,

λ_t is a penalty hyper-parameter, which balances the clean accuracy and the robustness.

Intuitively, TRADES minimizes the cross-entropy loss, while also regularizing for prediction smoothness in an δ -ball around each input.

2.2. Generalizing Robustness

Rice et al. [39] observe that the AT and TRADES methods may suffer from severe overfitting. Namely, the model exhibits higher robustness on the training data compared to the test data. A number of traditional strategies have been applied to alleviate the overfitting problem in robust training, such as ℓ_2 weight regularization, early stop [39], label smoothing, data augmentation [52, 54] and using synthetic data [22]. Below we describe popular and recent methods that were designed specifically for adversarial training.

Stochastic Weight Averaging (SWA). Izmailov et al. [25] introduces SWA for improved generalization performance in standard training. SWA maintains an exponential running average θ_{avg} of the model parameters θ at each training iteration and uses the running average θ_{avg} for inference. Namely,

$$\theta^{(t+1)} \leftarrow \text{SGD}(\theta^{(t)}); \quad \theta_{\text{avg}} \leftarrow \alpha\theta_{\text{avg}} + (1 - \alpha)\theta^{(t+1)}$$

where α is commonly set to 0.995. Recent work has also shown that SWA helps generalization in the robust training [22] scenario. Note that maintaining the running average requires additional memory resources.

Adversarial Weight Perturbation (AWP). Similar to Sharpness-Aware Minimization [16], Wu et al. [50] encourages model robustness by penalizing against the most offending local weight perturbation to the model. Specifically, given a robust loss $\hat{R}_*(\theta, D^m)$, AWP minimizes the following objective w.r.t θ :

$$\max_{\psi(\xi) \leq \delta_{\text{awp}}} \hat{R}_*(\theta + \xi, D^m) \quad (1)$$

where $*$ denotes either AT or T, ψ measures the amount of noise ξ (e.g. ℓ_2 norm) and δ_{awp} denotes the noise total budget. Note that solving the inner maximization problem requires at least one additional gradient ascent step in the parameter space.

Second-Order Statistic (S2O). Jin et al. [27] improve the robustness generalization by regularizing the statistical correlations between the weights of the network. Furthermore, they provide a second-order and data-dependent approximation A_θ of the weight correlation matrix. During training, S2O minimizes the following objective w.r.t θ :

$$\hat{R}_*(\theta, D^m) + \alpha \|A_\theta\|_F \quad (2)$$

where $\alpha > 0$ is a hyper-parameter. Computing A_θ involves computing the per-instance self-Kronecker product of the logit outputs for the clean and adversarial inputs.

2.3. PAC-Bayesian Theory for Robust Training

PAC-Bayesian theory [4, 9, 19, 35, 36, 43] provides a foundation for deriving an upper bound of the generalization gap between the training and test error. Both AWP and S2O plug the robust loss into the classical bound [36] to obtain the following form:

Theorem 1 (Square Root-Form PAC-Bayesian Bound [50])

Given a prior distribution \mathcal{P} on the weight θ of a network, any $\tau \in (0, 1]$, a robustness loss $R(\theta, \mathcal{D})$ for a data distribution \mathcal{D} and its empirical version $\hat{R}(\theta, D^m)$, for any posterior distribution \mathcal{Q} of θ , the following inequality holds with a probability at least $1 - \tau$,

$$\mathbb{E}_{\theta \in \mathcal{Q}} R(\theta, \mathcal{D}) \leq \mathbb{E}_{\theta \in \mathcal{Q}} \hat{R}(\theta, D^m) + 4\sqrt{\frac{1}{m} \text{KL}(\mathcal{Q} \parallel \mathcal{P}) + \log \frac{2m}{\tau}}. \quad (3)$$

Generally speaking, the goal of PAC-Bayesian learning is to optimize \mathcal{Q} on the RHS of Eq. 3 so as to obtain a tight upper bound on the test error (LHS). However, directly optimizing Eq. 3 over \mathcal{Q} is difficult because of the square root term. Instead of optimizing the RHS, AWP replaces it with $\max_{\xi} \hat{R}(\theta + \xi, D^m)$ plus a constant upper bound on the square root term, which is only loosely connected to the bound. On the other hand, S2O assumes \mathcal{P} and \mathcal{Q} as non-spherical Gaussian, i.e. $\mathcal{P} = \mathcal{N}(0, \Sigma_p)$, $\mathcal{Q} = \mathcal{N}(\theta, \Sigma_q)$ and show that the square root bound increases as the Frobenius norm and singular value of Σ_q increase. To overcome the complexity of the square root term, they approximate it with $\|A_\theta\|_F$ as in Eq. 2.

3. Direct PAC-Bayesian Bound Minimization

As mentioned earlier, neither AWP [50] nor S2O [27] minimize the PAC-Bayesian bound directly, likely due to the complicating square-root term in Eq. 3. However, Eq. 3 is only one instance out of PAC-Bayesian bounds defined in Germain et al. [19]. According to their framework, there is also a *linear-form* of the bound related to Bayesian inference which can be analytically minimized with the aid of a Gibbs distribution [13, 18, 41]. We leverage this linear-form of the PAC-Bayesian bound, and adapt it for bounding the robustness gap:

Theorem 2 (Linear-Form PAC-Bayesian Bound [18])

Under the same assumptions as in Theorem 1, for any $\beta > 0$, with a probability at least $1 - \tau$,

$$\mathbb{E}_{\theta \in \mathcal{Q}} R(\theta, \mathcal{D}) \leq \mathbb{E}_{\theta \in \mathcal{Q}} \hat{R}(\theta, D^m) + \frac{1}{\beta} \text{KL}(\mathcal{Q} \parallel \mathcal{P}) + C(\tau, \beta, m), \quad (4)$$

where $C(\tau, \beta, m)$ is a function independent of \mathcal{Q} .

Here β is a hyper-parameter that balances the three terms on the RHS. A common choice is $\beta \propto m$, i.e. the size of the dataset [14, 18]. Recently, [13] proposed to set \mathcal{P} and \mathcal{Q} to univariate Gaussians and used a second-order approximation to estimate the PAC-Bayesian bound. Applying a similar technique, we introduce Theorem 3 (see Appendix. A for the proof) which minimizes the RHS of Eq. 4.

Theorem 3 (Minimization of PAC-Bayesian Bound)

If $\mathcal{P} = \mathcal{N}(\mathbf{0}, \sigma_0^2)$, and \mathcal{Q} is also a product of univariate Gaussian distributions, then the minimum of Eq. 4 w.r.t \mathcal{Q} can be bounded by

$$\begin{aligned} & \min_{\mathcal{Q}} \mathbb{E}_{\theta \in \mathcal{Q}} R(\theta, \mathcal{D}) \\ & \leq \min_{\mathcal{Q}} \{ \mathbb{E}_{\theta \in \mathcal{Q}} \hat{R}(\theta, D^m) + \frac{1}{\beta} \text{KL}(\mathcal{Q} \parallel \mathcal{P}) \} + C(\tau, \beta, m) \\ & = \min_{\theta} \{ \hat{R}(\theta, D^m) + \frac{\|\theta\|_2^2}{2\beta\sigma_0^2} + \frac{\sigma_0^2}{2} \text{Tr}(\nabla_{\theta}^2 \hat{R}(\theta, D^m)) \} \\ & \quad + C(\tau, \beta, m) + O(\sigma_0^4). \end{aligned} \tag{5}$$

Assuming that $\sigma_0^2 = 1/d$ is the variance of the initial weight matrices where d is the input feature dimension, then $O(\sigma_0^4) = O(d^{-2})$. Theorem 3 considerably simplifies the optimization problem from one over the space of probability density functions \mathcal{Q} to one over model weights θ . Moreover, the resulting bound (RHS of Eq. 5) contains the Trace of Hessian (TrH) term $\text{Tr}(\nabla_{\theta}^2 \hat{R}(\theta, D^m))$ of the robust loss, which sums the loss surface curvatures in all directions. For a convex loss, the Hessian is positive semi-definite (PSD) in which case trace minimization leads θ to a flatter region of the loss surface. Although in general, our Hessian is not PSD, empirically we find that its largest eigenvalue has a much larger magnitude than the least ones [3] and that trace minimization correlates with minimizing the standard deviation of the eigenvalues (see Figure 5 in the appendix), so that the overall curvature is effectively decreases.

The RHS of Eq. 5 in Theorem 3 provides a training objective function that bounds the optimal test error up to a constant. However, evaluating and minimizing the bound in Eq. 5 requires computing the Trace of Hessian (TrH) term. Unfortunately, computing the Hessian directly by applying auto-differentiation twice is infeasible for a large deep network. Another solution is to apply Hutchinson’s method [5] to randomly approximate the TrH, however, the variance of the resulting estimator is too high and it ends up being too noisy for training in practice.

Instead, we propose to restrict TrH regularization to the top layer of the deep network only. Although this restriction brings approximation error to the bound, it has two benefits. First, the TrH on the top layer has simple analytical expressions for (Section 3.1). Second, we show that the top-layer TrH regularization effectively regularizes the TrH of the entire network as well (Section 3.2).

3.1. Top-Layer TrH regularizers for AT & TRADES

The network parameter θ can be decomposed into $\{\theta_t, \theta_b\}$ where θ_t denotes the weights of the top layer and θ_b denotes the weights of the remaining (lower) network. In this case, the logits can be expressed as $g_{\theta}(x) = \theta_t^{\top} f_{\theta_b}(x)$, where $f_{\theta_b}(x)$ is the penultimate layer feature. Furthermore, we define $h(x, \theta) = s(g_{\theta}(x)) - s(g_{\theta}(x'))^2$. Now, we present the analytical forms of the top-layer TrH w.r.t the AT and the TRADES in Proposition 1 and 2.

Proposition 1 (TrH for AT) Given a training dataset D^m and the adversarial input example x' for each example x , the top-layer TrH of the AT loss (Definition 1) is equal to

$$\begin{aligned} \text{Tr}(\nabla_{\theta_t}^2 \hat{R}_{AT}(\theta, D^m)) &= \frac{1}{m} \sum_{(x,y) \in D^m} \text{TrH}_{AT}(x'; \theta), \\ \text{where } \text{TrH}_{AT}(x'; \theta) &= \|f_{\theta_b}(x')\|_2^2 \cdot \mathbf{1}^{\top} h(x', \theta). \end{aligned}$$

Proposition 2 (TrH for TRADES) Under the same assumption in Proposition 1, the top-layer TrH of the TRADES loss (Definition 2) is equal to

$$\begin{aligned} \text{Tr}(\nabla_{\theta_t}^2 \hat{R}_T(\theta, D^m)) &= \frac{1}{m} \sum_{(x,y) \in D^m} \text{TrH}_T(x, x'; \lambda_t, \theta), \\ \text{where, } \text{TrH}_T(x, x'; \lambda_t, \theta) &= \|f_{\theta_b}(x)\|_2^2 \cdot \mathbf{1}^{\top} h(x, \theta) \\ & \quad + \lambda_t \|f_{\theta_b}(x')\|_2^2 \cdot \mathbf{1}^{\top} h(x', \theta). \end{aligned} \tag{6}$$

To obtain Eq. 6, we stopped the gradient on the KLloss in Definition 2 with respect to the clean logits $g_{\theta}(x)$, because we find it is more stable for training, otherwise, there would be an additional regularization term $G(x, x', \theta)$ in the TrH_T (see more details in the Appendix A).

With Proposition 1 and 2, we now present the complete training objective in Algorithm 1. Notice that, to simplify hyper-parameter notations, we re-parameterize $\gamma \stackrel{\text{def}}{=} 1/2\beta\sigma_0^2$ and $\lambda \stackrel{\text{def}}{=} \sigma_0^2/2$ in the algorithm.

3.2. The effect of Top-Layer TrH Regularization

Although the TrH regularization is restricted to the top layer only, the gradient back-propagates to the entire network through the penultimate layer features. This motivates the following research question:

What effect does top-layer TrH regularization have on the TrH of the entire network?

To answer this question, we take a two-step approach. First, we experiment with a small 3-layer network on the synthetic Two-Moon dataset (see Appendix B for a visualization of the dataset), provided that computing the full network Hessian is inexpensive. Subsequently, we provide a theorem that can be used to bound the Trace of Hessian of the full network with that of the top layer only.

Algorithm 1: TrH Regularization for Training Adversarial Robust Network

Hyper-parameters: The ℓ_2 -norm penalty for weights γ , the TRADES penalty λ_t and the TrH penalty λ .
Inputs: A batch B of examples, a `loss_type` = 'AT' or 'TRADES', the noise budget δ , and a network $g_\theta = \theta_t^\top f_{\theta_b}(x)$.
Output: The training objective at the current iteration.

```

1  $R \leftarrow 0$ ;
2 foreach  $(x, y) \in B$  do
3    $x' \leftarrow \text{PGD\_InnerLoop}(x, y, \delta, \text{loss\_type})$ 
4    $z' \leftarrow f_{\theta_b}(x')$ ,  $h' \leftarrow s(\theta_t^\top z') - s(\theta_t^\top z)$ ; //  $s$  is the softmax function. This step computes the
   penultimate feature  $z'$  and the softmax gradient  $h'$  on the adversarial input  $x'$ .
5   if loss_type == 'AT' then
6      $R \leftarrow R + \text{CE}((x', y), g_\theta) + \lambda(\|z'\|_2^2 \cdot \mathbf{1}^\top h')$ ;
7   else if loss_type == 'TRADES' then
8      $z \leftarrow f_{\theta_b}(x)$ ,  $h \leftarrow s(\theta_t^\top z) - s(\theta_t^\top z')$ ; // TRADES needs the  $z$  and  $h$  for the clean input  $x$ .
9      $R \leftarrow R + \text{CE}((x, y), g_\theta) + \lambda_t \text{KL}(s(\theta_t^\top z) \| s(\theta_t^\top z')) + \lambda(\|z\|_2^2 \cdot \mathbf{1}^\top h + \lambda_t \|z'\|_2^2 \cdot \mathbf{1}^\top h')$ ;
10  end
11 end
return:  $\frac{R}{|B|} + \gamma \|\theta\|_2^2$ 

```

Example 1 (Two Moons) We use 500 training examples, where $x \in \mathbb{R}^2$ and $y \in \{0, 1\}$ from the Two Moon dataset. We train a 3-layer fully-connected network with Dense(100)-ReLU-Dense(100)-ReLU-Dense(2) with the AT loss under three settings:

- *Standard:* no regularization.
- *Top:* Regularizing the TrH of the top layer only.
- *Full:* Regularizing the TrH of the entire network.

Throughout the training process (x-axis), we evaluate the TrH of the entire network (y-axis) with a numerical approach (twice differentiation) and plot the results in Figure 2.

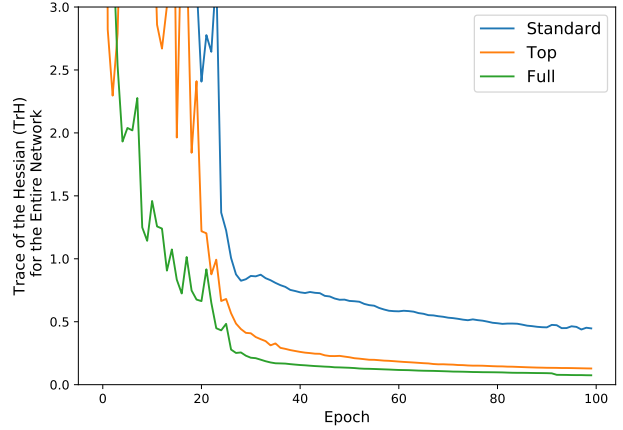


Figure 2. Trace of the Hessian (TrH) of the entire network (y-axis) over training epochs (x-axis) with (1) no regularization (Standard, in blue); (2) top layer TrH regularization (Top, in orange); and (3) regularization the TrH of all layers (Full, in green). See Example 1 for the experimental setup.

Figure 2 empirically shows that regularizing the TrH of the top layer (orange) indirectly reduces the TrH of the entire network and is nearly as effective as regularizing the entire network (green) after the 60-th epoch.

Next, we provide a theoretical justification for the impact of top-layer TrH regularization on the layers below. Intuitively, our Theorem 4, establishes an inductive relation between the TrH of the consecutive layers in a feedforward neural network with ReLU activation and CE loss, a common building block in AT and TRADES training.

Theorem 4 (Inductive Relation in TrH) Suppose g_θ is a feed-forward network with ReLU activation. For the i -th layer, let $W^{(i)}$ be its weight and $\mathcal{I}_x^{(i)}$ be its input evaluated at x . Thus, $\text{TrH}_x^{\text{CE}}(W^{(i-1)})$, i.e. TrH evaluated at x using a CE loss w.r.t $W^{(i-1)}$, is equal to

$$\text{TrH}_x^{\text{CE}}(W^{(i-1)}) = \|\{\mathcal{I}_x^{(i-1)}\}\|_2^2 \sum_{k,d \in P^{(i)}} \{\mathcal{H}^{(i)}\}_{k,d}$$

$$\text{where } \{\mathcal{H}^{(i)}\}_{k,d_i} \stackrel{\text{def}}{=} \left[\frac{\partial \{g_\theta(x)\}_k}{\partial \{\mathcal{I}_x^{(i)}\}_{d_i}} \right]^2 \cdot \{h(x, \theta)\}_k$$

$$P^{(i)} \stackrel{\text{def}}{=} \{d_i | \{\mathcal{I}_x^{(i)}\}_{d_i} > 0\}$$

and the following inequality holds for any $\mathcal{H}^{(i)}, \mathcal{H}^{(i+1)}$:

$$\max_{k,d_i} \{\mathcal{H}^{(i)}\}_{k,d_i} \leq \max_{k,d_{i+1}} \{\mathcal{H}^{(i+1)}\}_{k,d_{i+1}} \cdot \|W^{(i)}\|_1^2. \quad (7)$$

Put simply, the max-norm of the Hessian of each layer forms an upper bound for the max-norm of the layer below it (times a scalar). Therefore, regularizing the TrH of the top layer only implicitly regularizes the Hessian of the layers

below it. This effect explains the phenomenon observed in Example 1.

Furthermore, the operator norm $\|W^{(i)}\|_1^2$ of weights in Eq. 7 makes an interesting connection between TrH minimization and robust training. Roth et al. [40] show that robust training is an implicit way of regularizing the weight operator norm. Moreover, directly minimizing the operator norm is a commonly used technique in training certifiable robust networks [24, 32], a stronger version of the robustness guarantee targeted in this paper. Thus, the combination of robustness training and top-layer regularization results in an implicit regularization on TrH for internal layers.

4. Evaluation

In this section, we evaluate TrH regularization (Algorithm 1) over three image classification benchmarks including CIFAR-10/100 and ImageNet and compare against the robust training baselines described in Section 2.2.

4.1. Experiment Setup

Datasets and Threat Model. For CIFAR-10/100, we choose the standard $\epsilon = 0.031 (\approx 8/255)$ of the ℓ_∞ ball to bound the adversarial noise. In addition, Gowal et al. [22] has reported that using synthetic images from a DDPM [23] generator can improve the robustness accuracy for the original test set. Thus, we also add 1M DDPM images to CIFAR-10/100 (these images are publicly available [1]). For ImageNet, we choose $\epsilon = 3.0$ for the ℓ_2 and $\epsilon = 0.0157 (\approx 4/255)$ for the ℓ_∞ ball, respectively. We do not use extra data for ImageNet. The chosen ϵ s follow the common choices in the literature [22, 27, 33, 50]. We report the test accuracy evaluated with benign images and adversarial images generated by AutoAttack [11] (AutoPGD+AutoDLR), which is widely used in the literature [22, 27, 50].

Network Architectures. We use Vision Transformer (ViT) [15] through all experiments because of its success on multiple tasks over existing architectures. Specifically, we report the results of ViT-L16, Hybrid-L16 for CIFAR-10/100 and ViT-B16, ViT-L16 for ImageNet (additional results and architecture details can be found in Appendix F). We initialize the weights from a pre-trained checkpoint on ImageNet21K [2]. Notice that the resolution of the CIFAR images (32×32) are too small to correctly align with the pre-trained kernel of the first layer. To address this issue, we down-sample the kernel of the input layer following the receipt proposed by Mahmood et al. [34].

Methods. We train the models using AT and TRADES losses, together with the following defenses: (1) base: no regularization; (2) AWP [50]; (3) SWA [25]; (4) S2O [27]; and (5) our Algorithm 1 (TrH). We are interested in the

baselines defenses because of their connections to the PAC-Bayesian bound or the loss flatness. During training, the model was partitioned over four Google Cloud TPUv4 chips [28] for the base and TrH methods, and eight chips for AWP, S2O, and SWA as they consume more HBM memory.

Hyperparameter Selection. Training robust ViTs can be challenging due to a large number of hyper-parameters. We use two steps for hyperparameter selection. For the choice of common hyper-parameters, e.g. batch size, patch size, training iterations, and etc. (a full list is included in Appendix C), we first do a large grid search and select values that produce the best results on TRADES(base). This step is referred to as pre-tuning and is done per dataset.

After the first step, where the common hyper-parameters are locked, we tune and report the best results after trying different sets of method-specific hyper-parameters, e.g., the norm bound of weight noises in AWP and λ for TrH. Appendix D provides a full list of hyper-parameters we use to produce our main results in Table 1.

4.2. Main Results

In Table 1, we report the robust test accuracy using different types of defenses. The top results are highlighted in bold font. To measure the significance of an improvement, we calculate the maximum standard error (SE) [45] = $\sqrt{0.5 * (1 - 0.5) / m}$ (where m denotes the number of test examples) for each dataset. Thus, the accuracy of a certain model is regarded a *silver* result a_{silver} , if its SE interval overlaps with the that of the top result a_{top} . Namely, $a_{top} - SE \leq a_{silver} + SE$.

CIFAR-10/100. In CIFAR-10/100, a significant improvement is at least 1% according to SE. Therefore, based on Table 1, the performance differences among the methods are relatively small. Nevertheless, TrH attains either the top result (in 3 instances) or the silver result (in 5 instances) across all eight instances. In comparison, AWP is the second best with 3 top and 3 silver; S2O has 1 top and 4 silver; SWA has 3 silver; and the base has 1 top and 3 silver. Notably, Hybrid-L16+TRADES(TrH) achieves the highest robust accuracy (34.1%) on CIFAR-100 which beats all other baselines by at least 2%.

ImageNet. On ImageNet, a significant improvement is at least 0.4% according to SE. We observe that TrH regularization outperforms the other baselines across the board. Using AT(TrH), we set a new *state-of-the-art* robust accuracy of 48.8%, at $\ell_\infty(4/255)$ and 47.0% at $\ell_2(3.0)$ with a ViT-L16 model. Specifically, in the case of ℓ_∞ , 48.8% is an improvement of 4.7% compared to the basic setup AT(base). In TRADES(TrH), although the robust accuracy is even

$\ell_\infty(\delta = 8/255)$ SE= $\pm 0.5\%$ Defense	ViT-L16				Hybrid-L16			
	CIFAR-10		CIFAR-100		CIFAR-10		CIFAR-100	
	Clean(%)	AA(%)	Clean (%)	AA(%)	Clean(%)	AA(%)	Clean (%)	AA(%)
AT(base)	87.4	60.8	64.3	31.7	88.0	61.7	64.2	<u>31.8</u>
AT(SWA)	88.0	<u>61.7</u>	62.5	31.7	86.5	57.2	63.6	30.8
AT(S2O)	87.1	60.2	64.9	31.7	88.7	<u>61.6</u>	64.3	<u>31.8</u>
AT(AWP)	88.5	62.4	63.3	<u>32.6</u>	88.5	<u>61.5</u>	63.9	32.5
AT(TrH)	87.0	<u>61.7</u>	62.5	32.8	88.0	<u>61.0</u>	63.8	<u>32.4</u>
TRADES(base)	85.2	60.3	62.0	<u>31.4</u>	85.9	<u>60.8</u>	61.3	30.6
TRADES(SWA)	85.9	<u>60.7</u>	61.5	<u>32.0</u>	84.3	59.4	62.3	29.9
TRADES(S2O)	87.4	61.6	62.4	<u>31.6</u>	87.2	<u>61.5</u>	65.0	31.9
TRADES(AWP)	85.3	<u>60.8</u>	63.0	32.2	84.5	<u>59.8</u>	61.4	32.1
TRADES(TrH)	86.4	<u>61.4</u>	62.0	<u>32.1</u>	87.4	61.7	66.4	34.1

ImageNet	ViT-B16				ViT-L16			
	$\ell_\infty(\delta = 4/255)$		$\ell_2(\delta = 3.0)$		$\ell_\infty(\delta = 4/255)$		$\ell_2(\delta = 3.0)$	
	Clean(%)	AA(%)	Clean (%)	AA(%)	Clean(%)	AA(%)	Clean (%)	AA(%)
AT(base)	72.2	39.0	71.0	39.3	75.4	44.1	73.9	43.5
AT(SWA)	72.3	40.0	71.5	39.8	75.2	44.3	74.3	43.8
AT(S2O)	72.0	39.0	71.4	39.3	75.4	46.2	76.3	46.4
AT(AWP)	71.3	39.5	70.5	39.3	74.5	44.0	73.8	44.0
AT(TrH)	71.3	42.2	71.6	42.4	75.8	48.8	74.2	47.0
TRADES(base)	69.2	39.3	67.8	39.7	77.8	40.9	77.1	41.5
TRADES(SWA)	69.5	39.7	68.1	40.0	72.7	44.5	71.1	44.2
TRADES(S2O)	70.6	39.3	69.8	39.7	73.7	43.6	72.5	44.0
TRADES(AWP)	65.8	38.6	64.5	38.3	68.5	43.2	67.2	42.7
TRADES(TrH)	65.3	41.9	66.4	41.6	70.1	48.9	68.9	47.3

Table 1. Clean: % of Top-1 correct predictions. AA: % of Top-1 correct predictions under AutoAttack. A max Standard Error (SE) [45] = $\sqrt{0.5 * (1 - 0.5) / m}$ (m as the number of test examples) is computed for each dataset. The best results appear in bold. Underlined results are those that fall within the SE range of the result and are regarded roughly equal to the best result.

slightly higher than AT, the clean accuracy is lower. This is due to the choice of $\lambda_t = 6$, which strongly favors robustness over clean accuracy. As we reduce λ_t to 1, we obtain a better balance of (clean, AA) accuracy of TRADES(TrH) at (78.7, 46.7) for ℓ_∞ and (77.1, 45.2) for ℓ_2 .

Summary The results in Table 1 demonstrate that training with TrH regularization either matches or outperforms the robust accuracy of the existing methods. In fact, the gains of TrH regularization are wider on the larger ImageNet dataset compared to on CIFAR-10/100, where several methods show equivalent performance (per Standard Error analysis). This suggests that future work in robust adversarial training should move beyond the CIFAR benchmarks to larger-scale tasks.

4.3. Sensitivity and Efficiency

Sensitivity to λ . To study the sensitivity of λ to the training in TrH regularization, we train a ViT-L16 model over the ImageNet dataset and vary the choice of λ . Figure 3 plots the AA accuracy (y-axis) against the different choices of λ (x-axis) with all other setups fixed. The plot shows that $\lambda = 5 \times 10^{-4}$ attains the highest AA accuracy for both AT and TRADES losses with little degradation in the range of $[10^{-4}, 10^{-3}]$.

Training Efficiency. To compare the computational efficiency of the various methods, we report the peak memory usage and runtime performance (i.e., images processed per second; the higher the better) in Table 2. As the cloud TPU chips are dynamically allocated and pre-emptable, we instead measure these costs on two lo-

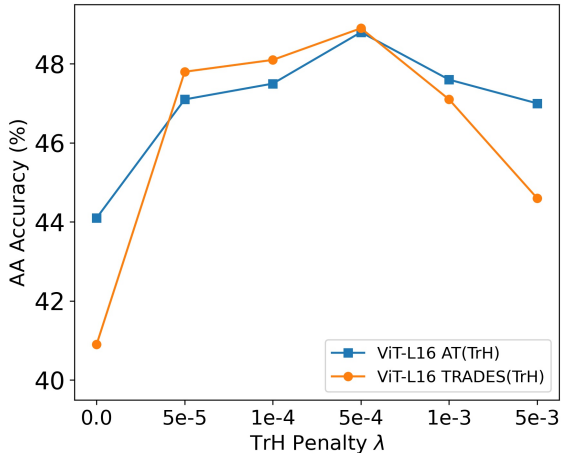


Figure 3. A plot of the Autoattack accuracy (AA %) against λ (TrH Penalty coefficient) when training on ImageNet with TrH Regularization in the ℓ_∞ case.

Defense	Mem.(MB/chip)	Img/sec/chip
AT(base)	5.0×10^3	5.5
AT(TrH) (ours)	5.0×10^3	5.2
AT(SWA)	5.6×10^3	4.4
AT(S2O)	8.0×10^3	5.2
AT(AWP)	6.8×10^3	3.7

Table 2. Peak memory usage and run-time reports measured when training CIFAR-10 using a ViT-L16 with a batch size of 32. Training is paralleled on two NVIDIA RTX chips. Lower memory usage and higher img/sec/chip are more efficient.

cal NVIDIA RTX chips with 24G memory per chip. Because by default JAX preallocates all GPUs, we set `XLA_PYTHON_CLIENT_ALLOCATOR=platform` before measuring the memory allocation and run-time. In Table 2, we show that adding TrH regularization brings almost no additional memory usage and runtime slowdown, compared to training without any regularization.

5. Related Work and Discussion

In this section, we situate our contributions in the broader context of current literature, such as related work on PAC-Bayesian theory, flatness regularization, as well as other types of robust adversarial losses.

PAC-Bayesian Theory and Flatness. Beyond the PAC-Bayesian inspired approaches for robust training that were already mentioned in the paper (such as Wu et al. [50]), a different line of work focuses on adapting PAC-Bayesian bounds for an ensemble of models, to improve either adver-

sarial robustness [46] or out-of-distribution (OOD) robustness data [53]. Several other works have focused on methods for finding flat local minima of the loss surface in order to improve (standard) model performance [13, 16, 26]. Also outside the scope of adversarial robustness, Ju et al. [29] find that trace of Hessian regularization leads to robustness against noise in the labels. Their Hessian regularization is based on randomized estimation and is done for all layers, whereas we effectively apply TrH regularization on the top layer only and with Theorem 4 as theoretical justification.

Perhaps the closest approach to ours is the PACTran-Gaussian metric [13], which uses a 2nd-order approximation of the PAC-Bayesian bound as the metric for evaluating the transferability of pretrained checkpoints. Similarly to our Eq. 5, the PACTran metric is composed of two terms: an ℓ_2 regularized empirical risk (RER) and a flatness regularizer (FR). Our work was inspired by the PACTran metric, but also makes several improvements. Firstly, in PACTran a single posterior variance σ_q^2 was shared for all parameters. On the contrary, we used different σ_q^2 's for different parameters. Secondly, in PACTran the optimization of the posterior mean θ_q is over the RER term only, while our optimization is over both RER and FR. These two changes potentially make our bound tighter than the one in the PACTran paper. In addition, we also study and explicitly include the high-order terms in $O(\sigma_0^4)$, which was neglected in PACTran.

Adversarial Surrogate Loss. In this paper, we focused only on the AT and TRADES approaches for robust adversarial optimization as they achieve reasonable results on the datasets of choice. In fact, recent work [22] on achieving state-of-the-art robustness on CIFAR-10 also exclusively focuses on AT or TRADES. Beyond AT and TRADES, the works in [12, 37, 47] explore other types of adversarial surrogate losses. Our method can be easily transferred to these losses and we include additional examples in Appendix G.

6. Conclusion

In summary, we alleviate overfitting in adversarial training with PAC-Bayesian theory. Using a linear-form PAC-Bayesian bound overlooked by the prior work, we derive a 2nd-order estimation that includes the Trace of Hessian (TrH) of the model. We then focus on the TrH of the top layer only, showing both empirically and theoretically (for ReLU networks) that its minimization effectively leads to the minimization of the TrH of the entire network, and thereby providing a sound flatness regularization technique for adversarial training which adds only little computational overhead. Experimental results show that our TrH regularization method is consistently among the top performers on CIFAR-10/100 benchmark as well as achieves a significant improvement in robust test accuracy on ImageNet compared to the other baselines.

References

- [1] Github - deepmind-research/adversarial_robustness. 6
- [2] Github - google-research/vision_transformer. 6
- [3] Guillaume Alain, Nicolas Le Roux, and Pierre-Antoine Manzagol. Negative eigenvalues of the hessian in deep neural networks, 2018. 4
- [4] Pierre Alquier. User-friendly introduction to pac-bayes bounds, 2021. 1, 3
- [5] Haim Avron and Sivan Toledo. Randomized algorithms for estimating the trace of an implicit symmetric positive semi-definite matrix. *J. ACM*, 58(2), apr 2011. 4
- [6] Nicholas Carlini and Hany Farid. Evading deepfake-image detectors with white- and black-box attacks. *2020 IEEE/CVF Conference on Computer Vision and Pattern Recognition Workshops (CVPRW)*, pages 2804–2813, 2020. 1
- [7] Nicholas Carlini and David Wagner. Towards evaluating the robustness of neural networks. In *2017 IEEE Symposium on Security and Privacy (SP)*, pages 39–57. Ieee, 2017. 1
- [8] Yair Carmon, Aditi Raghunathan, Ludwig Schmidt, John C Duchi, and Percy S Liang. Unlabeled data improves adversarial robustness. In *Advances in Neural Information Processing Systems*, volume 32. Curran Associates, Inc., 2019. 1
- [9] Olivier Catoni. A pac-bayesian approach to adaptive classification. 2004. 1, 3
- [10] Thomas Cilloni, Charles Walter, and Charles Fleming. Focused adversarial attacks. *ArXiv*, abs/2205.09624, 2022. 1
- [11] Francesco Croce and Matthias Hein. Reliable evaluation of adversarial robustness with an ensemble of diverse parameter-free attacks. In *International conference on machine learning*, pages 2206–2216. PMLR, 2020. 6
- [12] Gavin Weiguang Ding, Yash Sharma, Kry Yik Chau Lui, and Ruitong Huang. Mma training: Direct input space margin maximization through adversarial training. In *International Conference on Learning Representations*, 2020. 8
- [13] Nan Ding, Xi Chen, Tomer Levinboim, Beer Changpinyo, and Radu Soricut. Pactran: Pac-bayesian metrics for estimating the transferability of pretrained models to classification tasks. In *ECCV*, 2022. 2, 3, 4, 8
- [14] Nan Ding, Xi Chen, Tomer Levinboim, Sebastian Goodman, and Radu Soricut. Bridging the gap between practice and pac-bayes theory in few-shot meta-learning. In M. Ranzato, A. Beygelzimer, Y. Dauphin, P.S. Liang, and J. Wortman Vaughan, editors, *Advances in Neural Information Processing Systems*, volume 34, pages 29506–29516. Curran Associates, Inc., 2021. 4
- [15] Alexey Dosovitskiy, Lucas Beyer, Alexander Kolesnikov, Dirk Weissenborn, Xiaohua Zhai, Thomas Unterthiner, Mostafa Dehghani, Matthias Minderer, Georg Heigold, Sylvain Gelly, Jakob Uszkoreit, and Neil Houlsby. An image is worth 16x16 words: Transformers for image recognition at scale. In *International Conference on Learning Representations*, 2021. 2, 6, 25
- [16] Pierre Foret, Ariel Kleiner, Hossein Mobahi, and Behnam Neyshabur. Sharpness-aware minimization for efficiently improving generalization. In *International Conference on Learning Representations*, 2021. 3, 8
- [17] Pascal Germain, Francis Bach, Alexandre Lacoste, and Simon Lacoste-Julien. Pac-bayesian theory meets bayesian inference. In D. Lee, M. Sugiyama, U. Luxburg, I. Guyon, and R. Garnett, editors, *Advances in Neural Information Processing Systems*, volume 29. Curran Associates, Inc., 2016. 2
- [18] Pascal Germain, Francis Bach, Alexandre Lacoste, and Simon Lacoste-Julien. Pac-bayesian theory meets bayesian inference. In *Advances in Neural Information Processing Systems*, volume 29, 2016. 3, 4
- [19] Pascal Germain, Alexandre Lacasse, François Laviolette, and Mario Marchand. Pac-bayesian learning of linear classifiers. In *Proceedings of the 26th Annual International Conference on Machine Learning, ICML '09*, page 353–360, New York, NY, USA, 2009. Association for Computing Machinery. 1, 2, 3
- [20] Ian J. Goodfellow, Jonathon Shlens, and Christian Szegedy. Explaining and harnessing adversarial examples. *CoRR*, abs/1412.6572, 2015. 1
- [21] Sven Gowal, Chongli Qin, Jonathan Uesato, Timothy Mann, and Pushmeet Kohli. Uncovering the limits of adversarial training against norm-bounded adversarial examples, 2020. 1
- [22] Sven Gowal, Sylvestre-Alvise Rebuffi, Olivia Wiles, Florian Stimberg, Dan Andrei Calian, and Timothy Mann. Improving robustness using generated data. In *NeurIPS*, 2021. 1, 2, 3, 6, 8, 24
- [23] Jonathan Ho, Ajay Jain, and Pieter Abbeel. Denoising diffusion probabilistic models. *Advances in Neural Information Processing Systems*, 2020. 6
- [24] Yujia Huang, Huan Zhang, Yuanyuan Shi, J Zico Kolter, and Anima Anandkumar. Training certifiably robust neural networks with efficient local lipschitz bounds. In A. Beygelzimer, Y. Dauphin, P. Liang, and J. Wortman Vaughan, editors, *Advances in Neural Information Processing Systems*, 2021. 6
- [25] Pavel Izmailov, Dmitrii Podoprikin, Timur Garipov, Dmitry Vetrov, and Andrew Gordon Wilson. Averaging weights leads to wider optima and better generalization. In *34th Conference on Uncertainty in Artificial Intelligence 2018, UAI 2018*, 34th Conference on Uncertainty in Artificial Intelligence 2018, UAI 2018, pages 876–885. Association For Uncertainty in Artificial Intelligence (AUAI), 2018. 1, 2, 3, 6
- [26] Zhiwei Jia and Hao Su. Information-theoretic local minima characterization and regularization. In *Proceedings of the 37th International Conference on Machine Learning, ICML 2020, 13-18 July 2020, Virtual Event*, volume 119 of *Proceedings of Machine Learning Research*, pages 4773–4783. PMLR, 2020. 8
- [27] Gaojie Jin, Xinpeng Yi, Wei Huang, Sven Schewe, and Xiaowei Huang. Enhancing adversarial training with second-order statistics of weights. In *Proceedings of the IEEE/CVF Conference on Computer Vision and Pattern Recognition (CVPR)*, pages 15273–15283, June 2022. 1, 2, 3, 6
- [28] Norman P. Jouppi, Cliff Young, Nishant Patil, David A. Patterson, Gaurav Agrawal, Raminder Singh Bajwa, Sarah Bates, Suresh Bhatia, Nanette J. Boden, Al Borchers, Rick Boyle, Pierre luc Cantin, Clifford Chao, Chris Clark, Jeremy

- Coriell, Mike Daley, Matt Dau, Jeffrey Dean, Ben Gelb, Tara Vazir Ghaemmaghami, Rajendra Gottipati, William Gulland, Robert B. Hagmann, C. Richard Ho, Doug Hogberg, John Hu, Robert Hundt, Daniel Hurt, Julian Ibarz, Aaron Jaffey, Alek Jaworski, Alexander Kaplan, Harshit Khaitan, Daniel Killebrew, Andy Koch, Naveen Kumar, Steve Lacy, James Laudon, James Law, Diemthu Le, Chris Leary, Zhuyuan Liu, Kyle A. Lucke, Alan Lundin, Gordon MacKean, Adriana Maggiore, Maire Mahony, Kieran Miller, Rahul Nagarajan, Ravi Narayanaswami, Ray Ni, Kathy Nix, Thomas Norrie, Mark Omernick, Narayana Penukonda, Andy Phelps, Jonathan Ross, Matt Ross, Amir Salek, Emad Samadiani, Chris Severn, Gregory Sizikov, Matthew Snelham, Jed Souter, Dan Steinberg, Andy Swing, Mercedes Tan, Gregory Thorson, Bo Tian, Horia Toma, Erick Tuttle, Vijay Vasudevan, Richard Walter, Walter Wang, Eric Wilcox, and Doe Hyun Yoon. In-datacenter performance analysis of a tensor processing unit. *2017 ACM/IEEE 44th Annual International Symposium on Computer Architecture (ISCA)*, pages 1–12, 2017. [6](#)
- [29] Haotian Ju, Dongyue Li, and Hongyang R Zhang. Robust fine-tuning of deep neural networks with hessian-based generalization guarantees. In *Proceedings of the 39th International Conference on Machine Learning*, Proceedings of Machine Learning Research, pages 10431–10461. PMLR, 17–23 Jul 2022. [8](#)
- [30] Harini Kannan, Alexey Kurakin, and Ian J. Goodfellow. Adversarial logit pairing. *ArXiv*, abs/1803.06373, 2018. [26](#)
- [31] Alexey Kurakin, Ian J. Goodfellow, and Samy Bengio. Adversarial examples in the physical world. *ArXiv*, abs/1607.02533, 2017. [1](#)
- [32] Klas Leino, Zifan Wang, and Matt Fredrikson. Globally-robust neural networks. In *International Conference on Machine Learning*, pages 6212–6222. PMLR, 2021. [1](#), [6](#)
- [33] Aleksander Madry, Aleksandar Makelov, Ludwig Schmidt, Dimitris Tsipras, and Adrian Vladu. Towards deep learning models resistant to adversarial attacks. *arXiv preprint arXiv:1706.06083*, 2017. [1](#), [2](#), [6](#)
- [34] Kaleel Mahmood, Rigel Mahmood, and Marten van Dijk. On the robustness of vision transformers to adversarial examples. In *Proceedings of the IEEE/CVF International Conference on Computer Vision (ICCV)*, pages 7838–7847, October 2021. [6](#), [23](#), [26](#)
- [35] David A. McAllester. Pac-bayesian model averaging. In *COLT '99*, 1999. [1](#), [3](#)
- [36] Behnam Neyshabur, Srinadh Bhojanapalli, David McAllester, and Nati Srebro. Exploring generalization in deep learning. *Advances in neural information processing systems*, 30, 2017. [3](#)
- [37] Tianyu Pang, Min Lin, Xiao Yang, Junyi Zhu, and Shuicheng Yan. Robustness and accuracy could be reconcilable by (proper) definition. In *ICML*, 2022. [1](#), [8](#)
- [38] Siyuan Qiao, Huiyu Wang, Chenxi Liu, Wei Shen, and Alan Yuille. Micro-batch training with batch-channel normalization and weight standardization. *arXiv preprint arXiv:1903.10520*, 2019. [25](#)
- [39] Leslie Rice, Eric Wong, and J. Zico Kolter. Overfitting in adversarially robust deep learning. In *ICML*, 2020. [1](#), [3](#)
- [40] Kevin Roth, Yannic Kilcher, and Thomas Hofmann. Adversarial training is a form of data-dependent operator norm regularization. In H. Larochelle, M. Ranzato, R. Hadsell, M.F. Balcan, and H. Lin, editors, *Advances in Neural Information Processing Systems*, volume 33, pages 14973–14985. Curran Associates, Inc., 2020. [6](#)
- [41] Jonas Rothfuss, Vincent Fortuin, Martin Josifoski, and Andreas Krause. Pacoh: Bayes-optimal meta-learning with pac-guarantees. In *International Conference on Machine Learning*, pages 9116–9126. PMLR, 2021. [3](#)
- [42] Vikash Sehwal, Saeed Mahloujifar, Tinashe Handina, Sihui Dai, Chong Xiang, Mung Chiang, and Prateek Mittal. Robust learning meets generative models: Can proxy distributions improve adversarial robustness? In *ICLR*, 2022. [1](#)
- [43] John Shawe-Taylor and Robert C. Williamson. A pac analysis of a bayesian estimator. In *Proceedings of the Tenth Annual Conference on Computational Learning Theory*, COLT '97, page 2–9, New York, NY, USA, 1997. Association for Computing Machinery. [1](#), [3](#)
- [44] Dawn Song, Kevin Eykholt, Ivan Evtimov, Earlene Fernandes, Bo Li, Amir Rahmati, Florian Tramèr, Atul Prakash, and Tadayoshi Kohno. Physical adversarial examples for object detectors. In *12th USENIX Workshop on Offensive Technologies (WOOT 18)*, Baltimore, MD, Aug. 2018. USENIX Association. [1](#)
- [45] P.B. Stark and Berkeley. Department of Statistics University of California. *SticiGui: Statistics Tools for Internet and Classroom Instruction*. Department of Statistics. University of California, Berkeley, 2005. [6](#), [7](#), [27](#), [28](#)
- [46] Paul Viallard, Eric Guillaume VIDOT, Amaury Habrard, and Emilie Morvant. A pac-bayes analysis of adversarial robustness. In M. Ranzato, A. Beygelzimer, Y. Dauphin, P.S. Liang, and J. Wortman Vaughan, editors, *Advances in Neural Information Processing Systems*, volume 34, pages 14421–14433. Curran Associates, Inc., 2021. [8](#)
- [47] Yisen Wang, Difan Zou, Jinfeng Yi, James Bailey, Xingjun Ma, and Quanquan Gu. Improving adversarial robustness requires revisiting misclassified examples. In *International Conference on Learning Representations*, 2020. [1](#), [8](#), [29](#)
- [48] Xingxing Wei, Siyuan Liang, Xiaochun Cao, and Jun Zhu. Transferable adversarial attacks for image and video object detection. In *IJCAI*, 2019. [1](#)
- [49] Eric Wong, Frank Schmidt, Jan Hendrik Metzen, and J. Zico Kolter. Scaling provable adversarial defenses. In S. Bengio, H. Wallach, H. Larochelle, K. Grauman, N. Cesa-Bianchi, and R. Garnett, editors, *Advances in Neural Information Processing Systems*, volume 31. Curran Associates, Inc., 2018. [1](#)
- [50] Dongxian Wu, Shu-Tao Xia, and Yisen Wang. Adversarial weight perturbation helps robust generalization. In *NeurIPS*, 2020. [1](#), [2](#), [3](#), [6](#), [8](#), [25](#)
- [51] Yuxin Wu and Kaiming He. Group normalization. *International Journal of Computer Vision*, 128:742–755, 2019. [25](#)
- [52] Sangdoon Yun, Dongyoon Han, Seong Joon Oh, Sanghyuk Chun, Junsuk Choe, and Youngjoon Yoo. Cutmix: Regularization strategy to train strong classifiers with localizable features. In *Proceedings of the IEEE/CVF international conference on computer vision*, pages 6023–6032, 2019. [1](#), [3](#), [24](#)

- [53] Matteo Zecchin, Sangwoo Park, Osvaldo Simeone, Marios Kountouris, and David Gesbert. Robust pacm: Training ensemble models under model misspecification and outliers. *ArXiv*, abs/2203.01859, 2022. [8](#)
- [54] Hongyi Zhang, Moustapha Cisse, Yann N Dauphin, and David Lopez-Paz. mixup: Beyond empirical risk minimization. *arXiv preprint arXiv:1710.09412*, 2017. [1](#), [3](#)
- [55] Hongyang Zhang, Yaodong Yu, Jiantao Jiao, Eric Xing, Laurent El Ghaoui, and Michael Jordan. Theoretically principled trade-off between robustness and accuracy. In *International conference on machine learning*, pages 7472–7482. PMLR, 2019. [1](#), [2](#)

Appendix

A. Theorems and Proofs

A.1. Proof of Theorem 3

Theorem 3 If $\mathcal{P} = \mathcal{N}(\mathbf{0}, \sigma_0^2)$, and \mathcal{Q} is also a product of univariate Gaussian distributions, then the minimum of Eq. 4 w.r.t \mathcal{Q} can be bounded by

$$\begin{aligned} & \min_{\mathcal{Q}} \mathbb{E}_{\theta \in \mathcal{Q}} R(\theta, \mathcal{D}) \\ & \leq \min_{\mathcal{Q}} \{ \mathbb{E}_{\theta \in \mathcal{Q}} \hat{R}(\theta, D^m) + \frac{1}{\beta} \text{KL}(\mathcal{Q} || \mathcal{P}) \} + C(\tau, \beta, m) \\ & = \min_{\theta} \{ \hat{R}(\theta, D^m) + \frac{\|\theta\|_2^2}{2\beta\sigma_0^2} + \frac{\sigma_0^2}{2} \text{Tr}(\nabla_{\theta}^2 \hat{R}(\theta, D^m)) \} + C(\tau, \beta, m) + O(\sigma_0^4). \end{aligned}$$

Proof. Before we begin our proof, we emphasize that the posterior \mathcal{Q} that minimizes the test loss may not be the same posterior \mathcal{Q} that minimizes the training loss. Namely, define

$$\begin{aligned} \mathcal{Q}_{test} & \stackrel{\text{def}}{=} \arg \min_{\mathcal{Q}} \mathbb{E}_{\theta \in \mathcal{Q}} R(\theta, \mathcal{D}) \\ \mathcal{Q}_{train} & \stackrel{\text{def}}{=} \arg \min_{\mathcal{Q}} \{ \mathbb{E}_{\theta \in \mathcal{Q}} \hat{R}(\theta, D^m) + \frac{1}{\beta} \text{KL}(\mathcal{Q} || \mathcal{P}) \}, \end{aligned}$$

then \mathcal{Q}_{test} may not be equal to \mathcal{Q}_{train} . However, the following inequality clearly holds based on their definitions,

$$\mathbb{E}_{\theta \in \mathcal{Q}_{test}} R(\theta, \mathcal{D}) \leq \mathbb{E}_{\theta \in \mathcal{Q}_{train}} R(\theta, \mathcal{D}) \leq \mathbb{E}_{\theta \in \mathcal{Q}_{train}} \hat{R}(\theta, D^m) + \frac{1}{\beta} \text{KL}(\mathcal{Q} || \mathcal{P}) + C(\tau, \beta, m).$$

Generally speaking, it is impossible to directly find \mathcal{Q}_{test} without knowing the true data distribution \mathcal{D} . Thus, Theorem 3 attempts to derive \mathcal{Q}_{train} to minimize the RHS of Eq. 4. When it is clear which optimal posterior, i.e. \mathcal{Q}_{train} instead of \mathcal{Q}_{test} , we can derive in the theorem, we omit the subscription and directly write \mathcal{Q} .

Proof Overview. Based on our assumptions, we write $\mathcal{Q} = \mathcal{N}(\theta, \Sigma)$ where Σ is the (diagonal) covariance matrix. The minimization of the bound w.r.t \mathcal{Q} is to minimize the bound w.r.t Σ and θ . Our proof is therefore three-fold: (1) firstly, we write the expression of $\text{KL}(\mathcal{Q} || \mathcal{P})$ using θ and Σ ; (2) secondly, we use a second-order Taylor expansion to decompose $\mathbb{E}_{\theta \in \mathcal{Q}} \hat{R}(\theta, D^m)$ into terms as functions of Σ and θ ; and (3) finally, we minimize the bound w.r.t Σ for two cases: all weights have the same or different variances. Namely, the diagonal of Σ has the same or different elements. At the end of the minimization w.r.t Σ , we arrive at the bound that requires to minimize θ to actually minimize the RHS. Our proof follows below.

Extra Notations. Throughout the proof we will use N for the total number of weights, i.e. the cardinality of θ . When indexing a particular weight, we write θ_n . Let the diagonal of Σ be $\sigma^2 = [\sigma_1^2, \sigma_2^2, \dots, \sigma_N^2]^\top$, i.e. the variance of each weight. We use $\text{Diag}(a)$ to denote the diagonal matrix where the diagonal is the elements from vector a .

Step I: the KL term $\text{KL}(\mathcal{Q} || \mathcal{P})$. The expression of the KL term $\text{KL}(\mathcal{Q} || \mathcal{P})$ when $\mathcal{P} = \mathcal{N}(\mathbf{0}, \sigma_0^2 I)$ is as follows,

$$\begin{aligned} \text{KL}(\mathcal{Q} || \mathcal{P}) & = \frac{1}{2} \left[\log \frac{\sigma_0^2}{\det(\Sigma)} - N + \frac{\|\theta\|_2^2}{\sigma_0^2} + \frac{\text{Tr}(\Sigma)}{\sigma_0^2} \right] \\ & = \frac{1}{2} \left[\sum_n \log \frac{\sigma_0^2}{\sigma_n^2} - N + \frac{\|\theta\|_2^2}{\sigma_0^2} + \frac{\sum_n \sigma_n^2}{\sigma_0^2} \right] \quad (\text{when } \Sigma \text{ is a diagonal matrix}). \end{aligned} \quad (8)$$

Step II: Second-order Taylor's Expansion for $\mathbb{E}_{\theta \in \mathcal{Q}} \hat{R}(\theta, D^m)$. We expand $\mathbb{E}_{\theta \in \mathcal{Q}} \hat{R}(\theta, D^m)$ at the point θ and use the re-parameterization trick,

$$\begin{aligned}
\mathbb{E}_{\theta \in \mathcal{Q}} \hat{R}(\theta, D^m) &= \hat{R}(\theta, D^m) + \underbrace{\mathbb{E}_{\epsilon \sim \mathcal{N}(0, \Sigma)} [\epsilon^\top \nabla \hat{R}]}_{=0 \text{ because } \epsilon \text{ has zero mean}} + \frac{1}{2} \mathbb{E}_{\epsilon \sim \mathcal{N}(0, \Sigma)} [\epsilon^\top \nabla^2 \hat{R} \epsilon] \\
&+ \underbrace{\frac{1}{6} \mathbb{E}_{\epsilon \sim \mathcal{N}(0, \Sigma)} \left[\sum_{i,j,k} \frac{\partial^3 \hat{R}}{\partial \theta_i \theta_j \theta_k} \epsilon_i \epsilon_j \epsilon_k \right]}_{=0 \text{ because the mean and the skewness of a standard Gaussian are 0}} + O(\sigma^4) \\
&= \hat{R}(\theta, D^m) + \frac{1}{2} \mathbb{E}_{\epsilon \sim \mathcal{N}(0, I)} [(\sigma \circ \epsilon)^\top \nabla^2 \hat{R}(\sigma \circ \epsilon)] + O(\sigma^4)
\end{aligned} \tag{9}$$

where \circ is the element-wise product, a.k.a the Hadamard product. Notice the connection between a vector product and Hadamard product:

$$\text{for any vectors } a, b, \quad a \circ b = \text{Diag}(a)b. \tag{10}$$

Using Eq. 10, we simplify Eq. 9 as follows,

$$\begin{aligned}
\mathbb{E}_{\theta \in \mathcal{Q}} \hat{R}(\theta, D^m) &= \hat{R}(\theta, D^m) + \frac{1}{2} \mathbb{E}_{\epsilon \sim \mathcal{N}(0, I)} [(\text{Diag}(\sigma)\epsilon)^\top \nabla^2 \hat{R}(\text{Diag}(\sigma)\epsilon)] + O(\sigma^4) \\
&= \hat{R}(\theta, D^m) + \frac{1}{2} \text{Tr}(\Sigma \circ \nabla^2 \hat{R}) + O(\sigma^4).
\end{aligned} \tag{11}$$

Step III: Bound Minimization. Using Eq. 8 and 11, we re-write the bound in Theorem 2 as follows

$$\begin{aligned}
E_{\theta \in \mathcal{Q}} \hat{R}(\theta, D^m) &\leq \mathbb{E}_{\theta \in \mathcal{Q}} \hat{R}(\theta, D^m) + \frac{1}{\beta} \text{KL}(\mathcal{Q} \parallel \mathcal{P}) + C(\tau, \beta, m) \\
&= \hat{R}(\theta, D^m) + \frac{1}{2} \text{Tr}(\Sigma \circ \nabla^2 \hat{R}) + \frac{1}{2\beta} \left[\sum_n \log \frac{\sigma_0^2}{\sigma_n^2} - N + \frac{\|\theta\|_2^2}{\sigma_0^2} + \frac{\sum_n \sigma_n^2}{\sigma_0^2} \right] + O(\sigma^4) + C(\tau, \beta, m).
\end{aligned} \tag{12}$$

There are two sets of parameters in Eq. 12 for bound minimization: Σ (i.e. the σ^2) and θ . To minimize w.r.t Σ , strictly speaking it requires minimizing all relevant terms and the higher-order terms in $O(\sigma^4)$, which is clearly infeasible. Instead, we apply the following approximation by neglecting the higher-order $O(\sigma^4)$ and solve

$$\sigma^{*2} = \arg \min_{\sigma^2} \left\{ \hat{R}(\theta, D^m) + \frac{1}{2} \text{Tr}(\Sigma \circ \nabla^2 \hat{R}) + \frac{1}{2\beta} \left[\sum_n \log \frac{\sigma_0^2}{\sigma_n^2} - N + \frac{\|\theta\|_2^2}{\sigma_0^2} + \frac{\sum_n \sigma_n^2}{\sigma_0^2} \right] \right\}.$$

In the following, we discuss two cases of σ_n^2 .

Case I (Spherical Gaussian): $\forall n, \sigma_n^2 = \sigma_q^2$. In this case, the solution to the problem above is to take the derivative w.r.t. σ_q^2 and set it to zero. That is, for the optimal σ_q^{*2} ,

$$\text{Tr}(\hat{R}(\theta, D^m)) + \frac{K}{\beta} \left(\frac{1}{\sigma_0^2} - \frac{1}{\sigma_q^{*2}} \right) = 0 \implies \frac{\sigma_0^2}{\sigma_q^{*2}} = 1 + \frac{\sigma_0^2 \beta}{K} \text{Tr}(\hat{R}(\theta, D^m)).$$

Substituting each σ_n^2 with σ_q^{*2} in Eq. 12 gives the solution to the following problem

$$\min_{\sigma^2} \left[\mathbb{E}_{\theta \in \mathcal{Q}} \hat{R}(\theta, D^m) + \frac{1}{\beta} \text{KL}(\mathcal{Q} \parallel \mathcal{P}) \right] = \hat{R}(\theta, D^m) + \frac{K}{2\beta} \log \left(1 + \frac{\sigma_0^2 \beta}{K} \text{Tr}(\hat{R}(\theta, D^m)) \right) + \frac{\|\theta\|_2^2}{2\beta \sigma_0^2} + O(\sigma_q^{*4}).$$

With the Taylor expansion for $\log(1+x) = x + O(x^2)$,

$$\frac{K}{2\beta} \log \left(1 + \frac{\sigma_0^2 \beta}{K} \text{Tr}(\hat{R}(\theta, D^m)) \right) = \frac{\sigma_0^2}{2\beta} \text{Tr}(\hat{R}(\theta, D^m)) + O(\sigma_0^4) + O(\sigma_q^{*4}).$$

We can actually merge $O(\sigma_0^4) + O(\sigma_q^{*4})$ because

$$\frac{\sigma_0^2}{\sigma_q^{2*}} = 1 + \frac{\sigma_0^2 \beta}{K} \text{Tr}(\hat{R}(\theta, D^m)) \implies \sigma_0^2 \geq \sigma_q^{*2}$$

so $O(\sigma_0^4) + O(\sigma_q^{*4}) = O(\sigma_0^4)$. Lastly, to minimize the bound, we optimize it w.r.t θ , which leads us to land on:

$$\min_{\theta} \{ \hat{R}(\theta, D^m) + \frac{\|\theta\|_2^2}{2\beta\sigma_0^2} + \frac{\sigma_0^2}{2} \text{Tr}(\nabla_{\theta}^2 \hat{R}(\theta, D^m)) \} + C(\tau, \beta, m) + O(\sigma_0^4).$$

Case II (Diagonal): $\exists n_1, n_2, \sigma_{n_1}^2 \neq \sigma_{n_2}^2$. In this case, we take the derivative w.r.t each σ_n^2 and set it to zero. That is, for each optimal σ_n^{2*} ,

$$\frac{\partial \hat{R}^2}{\partial \theta_n^2} + \frac{1}{\beta} \left(\frac{1}{\sigma_0^2} - \frac{1}{\sigma_n^{2*}} \right) = 0 \implies \frac{\sigma_0^2}{\sigma_n^{2*}} = 1 + \sigma_0^2 \beta \frac{\partial \hat{R}^2}{\partial \theta_n^2}.$$

Substituting σ_n^2 with σ_n^{2*} in Eq. 12 gives the solution to the following problem

$$\min_{\sigma_n^2} \left[\mathbb{E}_{\theta \in \mathcal{Q}} \hat{R}(\theta, D^m) + \frac{1}{\beta} \text{KL}(\mathcal{Q} \parallel \mathcal{P}) \right] = \hat{R}(\theta, D^m) + \frac{1}{2\beta} \sum_n \log(1 + \sigma_0^2 \beta \frac{\partial \hat{R}^2}{\partial \theta_n^2}) + \frac{\|\theta\|_2^2}{2\beta\sigma_0^2} + O(\sigma^{*4}).$$

Similar to Case I, we take Taylor's Expansion of $\log(1+x)$ so

$$\frac{1}{2\beta} \sum_n \log(1 + \sigma_0^2 \beta \frac{\partial \hat{R}^2}{\partial \theta_n^2}) = \frac{\sigma_0^2}{2} \text{Tr}(\hat{R}(\theta, D^m)) + O(\sigma_0^4).$$

Lastly, using $O(\sigma_0^4) + O(\sigma^{*4}) = O(\sigma_0^4)$, we land on the same objective as derived in Case I:

$$\min_{\theta} \{ \hat{R}(\theta, D^m) + \frac{\|\theta\|_2^2}{2\beta\sigma_0^2} + \frac{\sigma_0^2}{2} \text{Tr}(\nabla_{\theta}^2 \hat{R}(\theta, D^m)) \} + C(\tau, \beta, m) + O(\sigma_0^4).$$

A.2. Proof of Theorem 4

Theorem 4 Suppose that g_{θ} is a feed-forward network with ReLU activation. For the i -th layer, let $W^{(i)}$ be its weight and $\mathcal{I}_x^{(i)} \in \mathbb{R}^{D^{(i)}}$ be its input evaluated at x . Thus, $\text{TrH}_x^{\text{CE}}(W^{(i-1)})$, i.e. TrH evaluated at x using a CE loss w.r.t $W^{(i-1)}$, is as follows

$$\text{TrH}_x^{\text{CE}}(W^{(i-1)}) = \|\{\mathcal{I}_x^{(i-1)}\}\|_2^2 \sum_{k,d \in P^{(i)}} \{\mathcal{H}^{(i)}\}_{k,d}$$

$$\text{where } \{\mathcal{H}^{(i)}\}_{k,d_i} \stackrel{\text{def}}{=} \left[\frac{\partial \{g_{\theta}(x)\}_k}{\partial \{\mathcal{I}_x^{(i)}\}_{d_i}} \right]^2 \cdot h_k(x, \theta)$$

$$P^{(i)} \stackrel{\text{def}}{=} \{d_i \mid \{\mathcal{I}_x^{(i)}\}_{d_i} > 0\}$$

and the following inequality holds for any $\mathcal{H}^{(i)}, \mathcal{H}^{(i+1)}$:

$$\max_{k,d_i} \{\mathcal{H}^{(i)}\}_{k,d_i} \leq \max_{k,d_{i+1}} \mathcal{H}^{(i+1)} \cdot \|W^{(i)}\|_1^2.$$

Proof. We use d_{i-1}, d_i and d_{i+1} to index the element of $\mathcal{I}_x^{(i-1)}, \mathcal{I}_x^{(i)}$ and $\mathcal{I}_x^{(i+1)}$. By the definition of trace, we need to compute the second-order derivative of the CE loss w.r.t to each entry in $W^{(i)}$. That is, we write

$$\text{TrH}_x^{\text{CE}}(W^{(i-1)}) = \sum_{d_{i-1}, d_i} \frac{\partial^2}{\partial W_{d_{i-1}, d_i}^{(i-1)2}} (\text{CE}((x, y), g_{\theta})). \quad (13)$$

First, we derive the first-order derivative. The following steps are based on the chain rule:

$$\begin{aligned}\frac{\partial}{\partial W_{d_{i-1}, d_i}^{(i-1)}}(CE((x, y), g_\theta)) &= \sum_k \frac{\partial}{\partial \{g_\theta(x)\}_k} (CE((x, y), g_\theta)) \cdot \frac{\{g_\theta(x)\}_k}{\partial W_{d_{i-1}, d_i}^{(i-1)}} \\ &= \sum_k (\{s(g_\theta(x))\}_k - y_k) \cdot \frac{\{g_\theta(x)\}_k}{\partial W_{d_{i-1}, d_i}^{(i-1)}}.\end{aligned}$$

The second-order derivative is therefore equal to

$$\begin{aligned}\frac{\partial^2}{\partial W_{d_{i-1}, d_i}^{(i-1)2}}(CE((x, y), g_\theta)) &= \sum_k \left(\frac{\partial}{\partial W_{d_{i-1}, d_i}^{(i-1)}} [\{s(g_\theta(x))\}_k - y_k] \cdot \frac{\{g_\theta(x)\}_k}{\partial W_{d_{i-1}, d_i}^{(i-1)}} + h_k(x, \theta) \cdot \frac{\partial}{\partial W_{d_{i-1}, d_i}^{(i-1)}} \left[\frac{\{g_\theta(x)\}_k}{\partial W_{d_{i-1}, d_i}^{(i-1)}} \right] \right) \\ &= \sum_k \left(h_k(x, \theta) \cdot \left[\frac{\{g_\theta(x)\}_k}{\partial W_{d_{i-1}, d_i}^{(i-1)}} \right]^2 + h_k(x, \theta) \cdot \frac{\partial}{\partial W_{d_{i-1}, d_i}^{(i-1)}} \left[\frac{\{g_\theta(x)\}_k}{\partial W_{d_{i-1}, d_i}^{(i-1)}} \right] \right).\end{aligned}$$

Notice that the first-order derivative of ReLU is either 1 or 0, so we have plenty of identity functions in $\frac{\{g_\theta(x)\}_k}{\partial W_{d_{i-1}, d_i}^{(i-1)}}$. Rigorously, ReLU does not have a second-order derivative. In practice, one will return 0 when querying the second-order derivative of ReLU. Thus, the following holds in practice.

$$\frac{\partial}{\partial W_{d_{i-1}, d_i}^{(i-1)}} \left[\frac{\partial \{g_\theta(x)\}_k}{\partial W_{d_{i-1}, d_i}^{(i-1)}} \right] = 0. \quad (14)$$

Eq. 14 simplifies the expression of the second-order derivative w.r.t $W_{d_{i-1}, d_i}^{(i-1)}$ so we have the following clean expression:

$$\begin{aligned}\frac{\partial^2}{\partial W_{d_{i-1}, d_i}^{(i-1)2}}(CE((x, y), g_\theta)) &= \sum_k \left[\frac{\partial \{g_\theta(x)\}_k}{\partial W_{d_{i-1}, d_i}^{(i-1)}} \right]^2 \cdot h_k(x, \theta) \\ &= \sum_k \left[\frac{\partial \{g_\theta(x)\}_k}{\partial \{\mathcal{I}_x^{(i)}\}_{d_i}} \cdot \frac{\partial \{\mathcal{I}_x^{(i)}\}_{d_i}}{\partial W_{d_{i-1}, d_i}^{(i-1)}} \right]^2 \cdot h_k(x, \theta) \\ &= \sum_k \left[\frac{\partial \{g_\theta(x)\}_k}{\partial \{\mathcal{I}_x^{(i)}\}_{d_i}} \cdot \mathbb{I}[\{\mathcal{I}_x^{(i)}\}_{d_i} > 0] \cdot \{\mathcal{I}_x^{(i-1)}\}_{d_{i-1}} \right]^2 \cdot h_k(x, \theta) \\ &= \mathbb{I}[\{\mathcal{I}_x^{(i)}\}_{d_i} > 0] \cdot \{\mathcal{I}_x^{(i-1)}\}_{d_{i-1}}^2 \cdot \sum_k \left[\frac{\partial \{g_\theta(x)\}_k}{\partial \{\mathcal{I}_x^{(i)}\}_{d_i}} \right]^2 \cdot h_k(x, \theta).\end{aligned} \quad (15)$$

By defining $\{\mathcal{H}^{(i)}\}_{k, d_i} \stackrel{\text{def}}{=} \left[\frac{\partial \{g_\theta(x)\}_k}{\partial \{\mathcal{I}_x^{(i)}\}_{d_i}} \right]^2 \cdot h_k(x, \theta)$, we further simplify Eq. 15 as follows

$$\frac{\partial^2}{\partial W_{d_{i-1}, d_i}^{(i-1)2}}(CE((x, y), g_\theta)) = \mathbb{I}[\{\mathcal{I}_x^{(i)}\}_{d_i} > 0] \cdot \{\mathcal{I}_x^{(i-1)}\}_{d_{i-1}}^2 \cdot \sum_k \{\mathcal{H}^{(i)}\}_{k, d_i}. \quad (16)$$

We plug Eq. 16 back to Eq. 13 and arrive

$$\begin{aligned}\text{TrH}_x^{\text{CE}}(W^{(i-1)}) &= \sum_{d_{i-1}, d_i} \mathbb{I}[\{\mathcal{I}_x^{(i)}\}_{d_i} > 0] \cdot \{\mathcal{I}_x^{(i-1)}\}_{d_{i-1}}^2 \cdot \sum_k \{\mathcal{H}^{(i)}\}_{k, d_i} \\ &= \left(\sum_{d_{i-1}} \{\mathcal{I}_x^{(i-1)}\}_{d_{i-1}}^2 \right) \cdot \sum_{k, d_i} \mathbb{I}[\{\mathcal{I}_x^{(i)}\}_{d_i} > 0] \cdot \{\mathcal{H}^{(i)}\}_{k, d_i} \\ &= \|\{\mathcal{I}_x^{(i-1)}\}\|_2^2 \cdot \sum_{k, d_i} \mathbb{I}[\{\mathcal{I}_x^{(i)}\}_{d_i} > 0] \cdot \{\mathcal{H}^{(i)}\}_{k, d_i}.\end{aligned}$$

By defining $P^{(i)}$ as a set of indices of positive neurons in $\mathcal{I}_x^{(i)}$, i.e., $\forall d_2 \in P^{(i)}, \{\mathcal{I}_x^{(i)}\}_{d_2} > 0$, we simplify the equation above as follows

$$\text{Tr}H_x^{\text{CE}}(W^{(i-1)}) = \|\{\mathcal{I}_x^{(i)}\}\|_2^2 \cdot \sum_{k, d_i \in P^{(i)}} \{\mathcal{H}^{(i)}\}_{k, d_i}.$$

Furthermore, by the definition of $\mathcal{H}^{(i)}$, we notice that

$$\begin{aligned} \{\mathcal{H}^{(i)}\}_{k, d_i} &= \left[\frac{\partial\{g_\theta(x)\}_k}{\partial\{\mathcal{I}_x^{(i)}\}_{d_i}} \right]^2 \cdot h_k(x, \theta) \\ &= \left\{ \sum_{d_{i+1}} \left[\frac{\partial\{g_\theta(x)\}_k}{\partial\{\mathcal{I}_x^{(i+1)}\}_{d_{i+1}}} \cdot \frac{\partial\{\mathcal{I}_x^{(i+1)}\}_{d_{i+1}}}{\partial\{\mathcal{I}_x^{(i)}\}_{d_i}} \right] \right\}^2 \cdot h_k(x, \theta) \end{aligned} \quad (17)$$

$$= \left\{ \sum_{d_{i+1}} \left[\left(\frac{\{\mathcal{H}^{(i+1)}\}_{k, d_{i+1}}}{h_k(x, \theta)} \right)^{\frac{1}{2}} \cdot \frac{\partial\{\mathcal{I}_x^{(i+1)}\}_{d_{i+1}}}{\partial\{\mathcal{I}_x^{(i)}\}_{d_i}} \right] \right\}^2 \cdot h_k(x, \theta). \quad (18)$$

Notice that the transition from Eq. 17 to Eq. 18 is because $\forall k, h_k(x, \theta) > 0$. Thus, we find

$$\{\mathcal{H}^{(i)}\}_{k, d_i} = \left\{ \sum_{d_{i+1}} \left[\{\mathcal{H}^{(i+1)}\}_{k, d_{i+1}}^{\frac{1}{2}} \cdot \frac{\partial\{\mathcal{I}_x^{(i+1)}\}_{d_{i+1}}}{\partial\{\mathcal{I}_x^{(i)}\}_{d_i}} \right] \right\}^2. \quad (19)$$

For each layer i , we denote $\mathcal{H}_{max}^{(i)} = \max_{k, d_i} \{\mathcal{H}^{(i)}\}_{k, d_i}$. Since $\forall i, d_i, \{\mathcal{H}^{(i)}\}_{k, d_i} > 0$, we can take the square root for $\mathcal{H}_{max}^{(i)}$ such that

$$\forall k, d_i, (\mathcal{H}_{max}^{(i)})^{\frac{1}{2}} \geq (\{\mathcal{H}^{(i)}\}_{k, d_i})^{\frac{1}{2}}.$$

Thus, we can bound $\{\mathcal{H}^{(i)}\}_{k, d_i}$ as follows:

$$\begin{aligned} \{\mathcal{H}^{(i)}\}_{k, d_i} &\leq \left\{ \sum_{d_{i+1}} \left[(\mathcal{H}_{max}^{(i+1)})^{\frac{1}{2}} \cdot \frac{\partial\{\mathcal{I}_x^{(i+1)}\}_{d_{i+1}}}{\partial\{\mathcal{I}_x^{(i)}\}_{d_i}} \right] \right\}^2 \\ &= \mathcal{H}_{max}^{(i)} \left[\sum_{d_{i+1}} \frac{\partial\{\mathcal{I}_x^{(i+1)}\}_{d_{i+1}}}{\partial\{\mathcal{I}_x^{(i)}\}_{d_i}} \right]^2. \end{aligned}$$

The squared term can be further bounded by using the chain rule, namely,

$$\begin{aligned} \{\mathcal{H}^{(i)}\}_{k, d_i} &\leq \mathcal{H}_{max}^{(i+1)} \left[\sum_{d_{i+1}} \mathbb{I}[\{\mathcal{I}_x^{(i+1)}\}_{d_{i+1}} > 0] \cdot W_{d_i, d_{i+1}}^{(i)} \right]^2 \\ &\leq \mathcal{H}_{max}^{(i+1)} \left[\sum_{d_{i+1}} |W_{d_i, d_{i+1}}^{(i)}| \right]^2. \end{aligned}$$

Recall that our goal is to bound $\mathcal{H}_{max}^{(i)}$. By definition, we take the max on both sides over d_i and k (although the class dimension is already gone). The direction of the inequality still holds because quantities on both sides are all non-negative.

$$\mathcal{H}_{max}^{(i)} \leq \mathcal{H}_{max}^{(i+1)} \max_{d_i} \left[\sum_{d_{i+1}} |W_{d_i, d_{i+1}}^{(i)}| \right]^2.$$

The order of max and square can be exchanged because $|W_{d_i, d_{i+1}}^{(i)}|$ is non-negative. Thus,

$$\mathcal{H}_{max}^{(i)} \leq \mathcal{H}_{max}^{(i+1)} \left[\max_{d_i} \sum_{d_{i+1}} |W_{d_i, d_{i+1}}^{(i)}| \right]^2.$$

The last term inside the square is the definition of the ℓ_1 operator norm so we directly write

$$\mathcal{H}_{max}^{(i)} \leq \mathcal{H}_{max}^{(i+1)} \cdot \|W^{(i)}\|_1^2.$$

A.3. Derivations of Propositions

Proposition 1 Given a training dataset D^m and the adversarial input example x' for each example x , the top-layer TrH of the AT loss (Definition 1) is equal to

$$\begin{aligned} \text{Tr}(\nabla_{\theta_t}^2 \hat{R}_{\text{AT}}(\theta, D^m)) &= \frac{1}{m} \sum_{(x, y) \in D^m} \text{TrH}_{\text{AT}}(x'; \theta), \\ \text{where } \text{TrH}_{\text{AT}}(x'; \theta) &= \|f_{\theta_b}(x')\|_2^2 \cdot \mathbf{1}^\top h(x', \theta). \end{aligned}$$

Proof. We firstly write the expression of $\hat{R}_{\text{AT}}(\theta, D^m)$ based on Definition 1,

$$\hat{R}_{\text{AT}}(\theta, D^m) = \frac{1}{m} \sum_{(x, y) \in D^m} \max_{\|\epsilon\|_p \leq \delta} \text{CE}((x + \epsilon, y), F_\theta).$$

Let x' be an adversarial example, namely

$$x' = \arg \max_{\|\epsilon\|_p \leq \delta} [\text{CE}((x, y), F_\theta)] + x.$$

AT loss can be simplified as

$$\hat{R}_{\text{AT}}(\theta, D^m) = \frac{1}{m} \sum_{(x, y) \in D^m} \text{CE}((x', y), F_\theta) = \frac{1}{m} \sum_{(x, y) \in D^m} \sum_k -y_k \log s(g'_k),$$

where $g'_k = \{\theta_t^\top f_{\theta_b}(x')\}_k$ is the logit score of class k at the adversarial example x' and $s(\cdot)$ is the softmax function. Let's consider the loss at each adversarial point

$$R = \sum_k -y_k \log s(g'_k).$$

We want to compute the derivatives of R with respect to the weight at the top layer $\{\theta_t\}_{jk}$. For the ease of the notation, let's define $w = \theta_t$ so $w_{jk} = \{\theta_t\}_{jk}$ and $\nabla_{w_{jk}} R$ is equal to

$$\nabla_{w_{jk}} R = \sum_k -y_k \nabla_{w_{jk}} [\log s(g'_k)] = \{f_{\theta_b}(x')\}_j (s(g'_k) - y_k). \quad (20)$$

The transition to Eq. 20 uses the standard form of the gradient of Cross Entropy loss with the softmax activation. To compute the trace of a Hessian, we can skip the cross terms in Hessian (e.g. $\nabla_{w_{j_1 k}, w_{j_2 k}} R$) because they are not on the diagonal of the matrix. Thus, we are only interested in $\nabla_{w_{jk}}^2 R$, which are

$$\begin{aligned} \nabla_{w_{jk}}^2 R &= \nabla_{w_{jk}} [\nabla_{w_{jk}} R] = \nabla_{w_{jk}} [x'_j (s(g'_k) - y_k)] \\ &= \{f_{\theta_b}(x')\}_j \cdot \{f_{\theta_b}(x')\}_j \cdot s(g'_k) (1 - s(g'_k)) \\ &= \{f_{\theta_b}(x')\}_j^2 (s(g'_k) - s^2(g'_k)). \end{aligned}$$

Eventually, to compute the trace of Hessian matrix we sum all diagonal terms so that

$$\text{Tr}(\nabla_{w_{jk}}^2 R) = \sum_{j, k} \nabla_{w_{jk}}^2 R = \sum_{j, k} \{f_{\theta_b}(x')\}_j^2 (s(g'_k) - s^2(g'_k)) = \|f_{\theta_b}(x')\|_2^2 \cdot \mathbf{1}^\top h(x', \theta)$$

and we denote $\text{Tr}(\nabla_{w_{jk}}^2 R)$ as $\text{TrH}_{\text{AT}}(x'; \theta)$ to complete the proof.

Proposition 2 Under the same assumption as in Proposition 1, the top-layer TrH of the TRADES loss (Def' 2) is equal to

$$\text{Tr}(\nabla_{\theta_t}^2 \hat{R}_{\text{T}}(\theta, D^m)) = \frac{1}{m} \sum_{(x,y) \in D^m} \text{TrH}_{\text{T}}(x, x'; \lambda_t, \theta),$$

where, $\text{TrH}_{\text{T}}(x, x'; \lambda_t, \theta) = \|f_{\theta_b}(x)\|_2^2 \cdot \mathbf{1}^{\top} h(x, \theta) + \lambda_t \|f_{\theta_b}(x')\|_2^2 \cdot \mathbf{1}^{\top} h(x', \theta)$.

Before we start our proof of this proposition, we introduce the following useful lemmas.

Lemma 1 Let $s(g)$ be the softmax output of the logit output g computed at input x , then

$$\frac{\partial s(g)}{\partial g} = \Phi = \text{diag}[s(g)] - s(g) \cdot \{s(g)\}^{\top} \quad (21)$$

where $\text{diag}(v)$ returns an identity matrix with its diagonal replaced by a vector v .

Proof.

$$\frac{\partial s(g_i)}{\partial g_k} = s(g_i)(\mathbb{I}[i = k] - s(g_k)), \Phi_{ik} = s(g_i) \cdot \mathbb{I}[i = k] - s(g_i)s(g_k) \implies \frac{\partial s(g)}{\partial g} = \Phi.$$

Lemma 2 Let $\log s(g(x))$ be the log softmax output of the logit output g computed at input x , then

$$\frac{\partial \log s(g(x))}{\partial g(x)} = \Psi = I - \mathbf{1} \cdot \{s(g(x))\}^{\top}$$

where I is the identity matrix.

Proof.

$$\frac{\partial \log s(g_i)}{\partial g_k} = \mathbb{I}[i = k] - s(g_k), \Psi_{ik} = \mathbb{I}[i = k] - s(g_k) \implies \frac{\partial s(g)}{\partial g} = \Psi.$$

Now we are ready to present our proof of the Proposition 2.

Proof. We write the expression of $\hat{R}_{\text{T}}(\theta, D^m)$ based on as Definition 2.

$$\hat{R}_{\text{T}}(\theta, D^m) \stackrel{\text{def}}{=} \frac{1}{m} \sum_{(x,y) \in D^m} \left[\text{CE}((x, y), g_{\theta}) + \lambda_t \cdot \max_{\|\epsilon\|_p \leq \delta} \text{KLloss}((x, x + \epsilon), g_{\theta}) \right],$$

where $\text{KLloss}((x, x + \epsilon), g_{\theta}) = \text{KL}(s(g_{\theta}(x)) \| s(g_{\theta}(x + \epsilon)))$. Thus, we can compute the trace of Hessian on the top layer for the CE loss and the KL loss, respectively. Namely, we derive $\nabla_{\theta_t}^2 [\text{CE}((x, y), F_{\theta})]$ and $\nabla^2 [\max_{\|\epsilon\|_p \leq \delta} \text{KLloss}((x, x + \epsilon), F_{\theta})]$.

First, we see that the expression of $\nabla_{\theta_t}^2 [\text{CE}((x, y), F_{\theta})]$ is similar to the result in Proposition 1 by replacing the adversarial input with the clean input. With this similarity, we directly write

$$\text{Tr}\{\nabla_{\theta_t}^2 [\text{CE}((x, y), F_{\theta})]\} = \|f_{\theta_b}(x)\|_2^2 \cdot \mathbf{1}^{\top} h(x, \theta). \quad (22)$$

Second, by denoting

$$x' = \arg \max_{\|\epsilon\|_p \leq \delta} [\text{KLloss}((x, x + \epsilon), F_{\theta})] + x,$$

the rest of the proof now focuses on deriving $\nabla_{\theta_t}^2 [\text{KLloss}((x, x'), F_{\theta})]$ where

$$\text{KLloss}((x, x'), F_{\theta}) = - \sum_i s(g_i) \log(s(g'_i)) + \left[\sum_i s(g_i) \log(s(g_i)) \right], \quad g_i = \{\theta_t^{\top} f_{\theta_b}(x)\}_i, g'_i = \{\theta_t^{\top} f_{\theta_b}(x')\}_i.$$

For the ease of the notation, let $w \stackrel{\text{def}}{=} \theta_t$ so $w_{jk} \stackrel{\text{def}}{=} \{\theta_t\}_{jk}$ and let $K \stackrel{\text{def}}{=} \text{KLloss}((x, x'), F_{\theta})$. To find $\nabla_{\theta_t}^2 K$, we first write the first-order derivative of K with respect to w ,

$$\frac{\partial K}{\partial w_{jk}} = - \sum_i s(g_i) \frac{\partial}{\partial g'_k} [\log(s(g'_i))] \frac{\partial g'_k}{\partial w_{jk}} + \underbrace{\sum_i \frac{\partial K}{\partial s(g_i)} \frac{\partial s(g_i)}{\partial g_k} \frac{\partial g_k}{\partial w_{jk}}}_{\text{gradient through } g_k}. \quad (23)$$

Next, we discuss two cases depending on whether or not we stop gradient on g (the logit output of the clean input) in Eq. 23. In Case I where the gradient on g is stopped, the second term of Eq. 23 will vanish. This leads to a simpler but practically more stable objective function.

Case I: Stop Gradient on g . In this case,

$$\begin{aligned}\frac{\partial K}{\partial w_{jk}} &= -\sum_i s(g_i) \frac{\partial}{\partial g'_k} [\log(s(g'_i))] \frac{\partial g'_k}{\partial w_{jk}} \\ &= \{f_{\theta_b}(x')\}_j (s(g'_k) - s(g_k)).\end{aligned}\quad (24)$$

By comparing Eq. 24 with Eq. 20 and treating $s(g_k)$ as constants, we can quickly write out the second-order derivative as

$$\frac{\partial^2 K}{\partial w_{jk}^2} = \{f_{\theta_b}(x')\}_j^2 (s(g'_k) - s^2(g'_k)).$$

Recalling $h(x', \theta) = s(g') - s^2(g')$, therefore,

$$\text{Tr}\{\nabla_{\theta_t}^2 [\text{KLloss}((x, x'), F_\theta)]\} = \text{Tr}\{\nabla_{\theta_t}^2 K\} = \sum_{jk} \frac{\partial^2 K}{\partial w_{jk}^2} = \|f_{\theta_b}(x')\|_2^2 \cdot \mathbf{1}^\top h(x', \theta). \quad (25)$$

Finally, we combine Eq. 22 and 25 to arrive at

$$\begin{aligned}\text{Tr}\left\{\nabla_{\theta_t}^2 \left[\text{CE}((x, y), g_\theta) + \lambda_t \cdot \max_{\|\epsilon\|_p \leq \delta} \text{KLloss}((x, x + \epsilon), g_\theta)\right]\right\} &= \|f_{\theta_b}(x)\|_2^2 \cdot \mathbf{1}^\top h(x, \theta) + \lambda_t \|f_{\theta_b}(x')\|_2^2 \cdot \mathbf{1}^\top h(x', \theta), \\ \text{where } x' &= \arg \max_{\|\epsilon\|_p \leq \delta} [\text{KLloss}((x, x + \epsilon), F_\theta)] + x\end{aligned}$$

By denoting $\text{TrH}_\perp(x, x'; \lambda_t, \theta) \stackrel{\text{def}}{=} \text{Tr}\left\{\nabla_{\theta_t}^2 \left[\text{CE}((x, y), g_\theta) + \lambda_t \cdot \max_{\|\epsilon\|_p \leq \delta} \text{KLloss}((x, x + \epsilon), g_\theta)\right]\right\}$, we complete the proof for this case and this is the statement shown in Proposition 2.

Case II: With Gradient on g . We restart our derivation from Eq. 23 and expand the first term as follows

$$\frac{\partial K}{\partial w_{jk}} = \{f_{\theta_b}(x')\}_j (s(g'_k) - s(g_k)) + \sum_i \frac{\partial K}{\partial s(g_i)} \frac{\partial s(g_i)}{\partial g_k} \frac{\partial g_k}{\partial w_{jk}}.$$

Here

$$\sum_i \frac{\partial K}{\partial s(g_i)} \frac{\partial s(g_i)}{\partial g_k} \frac{\partial g_k}{\partial w_{jk}} = -\{f_{\theta_b}(x)\}_j \sum_i \frac{\partial s(g_i)}{\partial g_k} \log s(g'_i) + \{f_{\theta_b}(x)\}_j \sum_i \left[\frac{\partial s(g_i)}{\partial g_k} \log s(g_i) + s(g_i) \frac{\partial \log s(g_i)}{\partial g_k} \right]$$

Using Lemma 1 and 2, we write

$$\frac{\partial s(g_i)}{\partial g_k} = \Phi_{ik}, \quad \frac{\partial \log s(g_i)}{\partial g_k} = \Psi_{ik}, \quad \Phi_{ik} = s(g_i) \Psi_{ik}$$

and

$$\sum_i \frac{\partial K}{\partial s(g_i)} \frac{\partial s(g_i)}{\partial g_k} \frac{\partial g_k}{\partial w_{jk}} = -\{f_{\theta_b}(x)\}_j \sum_i \Phi_{ik} \log s(g'_i) + \{f_{\theta_b}(x)\}_j \sum_i [\Phi_{ik} \log s(g_i) + \Phi_{ik}].$$

Therefore, the first-order derivative of K with respect to w_{jk} is

$$\begin{aligned}\frac{\partial K}{\partial w_{jk}} &= \{f_{\theta_b}(x')\}_j (s(g'_k) - s(g_k)) - \{f_{\theta_b}(x)\}_j \sum_i \Phi_{ik} \log s(g'_i) + \{f_{\theta_b}(x)\}_j \sum_i [\Phi_{ik} \log s(g_i) + \Phi_{ik}] \\ &= \underbrace{\{f_{\theta_b}(x')\}_j s(g'_k)}_{K'} - \underbrace{\{f_{\theta_b}(x')\}_j s(g_k)}_{K_1} - \underbrace{\{f_{\theta_b}(x)\}_j \sum_i \Phi_{ik} \log s(g'_i)}_{K_2} + \underbrace{\{f_{\theta_b}(x)\}_j \sum_i [\Phi_{ik} \log s(g_i) + \Phi_{ik}]}_{K_3}.\end{aligned}$$

To calculate the seconder-order derivative of K w.r.t w_{jk} , we find the derivative of K', K_1, K_2, K_3 w.r.t w_{jk} , respectively.

(1) **Derivative of K' .** K' is simply the result we have already obtained in Case I (see Eq. 24); therefore,

$$\frac{\partial K'}{\partial w_{jk}} = \{f_{\theta_b}(x')\}_j^2 (s(g'_k) - s^2(g'_k)).$$

Thus,

$$\text{Tr}\left(\frac{\partial K'}{\partial w_{jk}}\right) = \|f_{\theta_b}(x')\|_2^2 \cdot \mathbf{1}^\top h(x', \theta).$$

(2) **Derivative of K_1 .**

$$\begin{aligned} \frac{\partial K_1}{\partial w_{jk}} &= -\{f_{\theta_b}(x')\}_j \{f_{\theta_b}(x)\}_j \frac{\partial s(g_k)}{\partial g_k} \\ &= -\{f_{\theta_b}(x')\}_j \{f_{\theta_b}(x)\}_j \Phi_{kk} \\ &= -\{f_{\theta_b}(x')\}_j \{f_{\theta_b}(x)\}_j (s(g_k) - s^2(g_k)). \end{aligned}$$

Thus,

$$\begin{aligned} \text{Tr}\left(\frac{\partial K_1}{\partial w_{jk}}\right) &= -\sum_{jk} \{f_{\theta_b}(x')\}_j \{f_{\theta_b}(x)\}_j (s(g_k) - s^2(g_k)) \\ &= -f_{\theta_b}(x')^\top f_{\theta_b}(x) \cdot \mathbf{1}^\top h(x, \theta) \end{aligned}$$

(3) **Derivative of K_2 .**

$$\begin{aligned} \frac{\partial K_2}{\partial w_{jk}} &= -\{f_{\theta_b}(x)\}_j \sum_i \left[\frac{\partial \Phi_{ik}}{\partial g_k} \frac{\partial g_k}{\partial w_{jk}} \log s(g'_i) + \Phi_{ik} \frac{\partial \log s(g'_i)}{\partial g'_k} \frac{\partial g'_k}{\partial w_{jk}} \right] \\ &= -\{f_{\theta_b}(x)\}_j \sum_i \left[\frac{\partial \Phi_{ik}}{\partial g_k} \{f_{\theta_b}(x)\}_j \log s(g'_i) + \Phi_{ik} \Psi'_{ik} \{f_{\theta_b}(x')\}_j \right] \end{aligned}$$

Notice that

$$\begin{aligned} i = k &\implies \frac{\partial \Phi_{ik}}{\partial g_k} = \frac{\partial \Phi_{kk}}{\partial g_k} = \frac{\partial}{\partial g_k} (s(g_k) - s^2(g_k)) = \Phi_{kk} - 2s(g_k)\Phi_{kk}; \\ \text{and } i \neq k &\implies \frac{\partial \Phi_{ik}}{\partial g_k} = \frac{\partial}{\partial g_k} (-s(g_i)s(g_k)) = -2s(g_i)\Phi_{kk}. \end{aligned}$$

Thus,

$$\frac{\partial \Phi_{ik}}{\partial g_k} = \Phi_{kk} (\mathbb{I}[k=i] - s(g_i)) = \Phi_{kk} \{\Psi^\top\}_{ik} = \Phi_{kk} \Psi_{ki}.$$

As a result,

$$\begin{aligned} \frac{\partial K_2}{\partial w_{jk}} &= -\{f_{\theta_b}(x)\}_j \sum_i [\Phi_{kk} \Psi_{ki} \{f_{\theta_b}(x)\}_j \log s(g'_i) + \Phi_{ik} \Psi'_{ik} \{f_{\theta_b}(x')\}_j] \\ &= -\{f_{\theta_b}(x)\}_j^2 \Phi_{kk} \sum_i \Psi_{ki} \log s(g'_i) - \{f_{\theta_b}(x)\}_j \{f_{\theta_b}(x')\}_j \sum_i \Phi_{ik} \Psi'_{ik} \\ &= (-\{f_{\theta_b}(x)\}_j^2 \Phi_{kk}) (\Psi_k \cdot \log s(g')) - \{f_{\theta_b}(x)\}_j \{f_{\theta_b}(x')\}_j (\{\Phi^\top\}_k \cdot \{\Psi'^\top\}_k). \end{aligned}$$

Thus,

$$\begin{aligned} \text{Tr}\left(\frac{\partial K_2}{\partial w_{jk}}\right) &= \sum_{jk} [(-\{f_{\theta_b}(x)\}_j^2 \Phi_{kk}) (\Psi_k \cdot \log s(g')) - \{f_{\theta_b}(x)\}_j \{f_{\theta_b}(x')\}_j (\{\Phi^\top\}_k \cdot \{\Psi'^\top\}_k)] \\ &= -\|f_{\theta_b}(x)\|_2^2 \cdot \psi'^\top h(x, \theta) - f_{\theta_b}(x')^\top f_{\theta_b}(x) \cdot \mathbf{1}^\top \omega', \end{aligned}$$

where ψ', ω' are vectors such that $\psi'_k = \Psi_k \cdot \log s(g')$, $\omega'_k = \{\Phi^\top\}_k \cdot \{\Psi'^\top\}_k$.

(4) Derivative of K_3 .

$$\begin{aligned}
\frac{\partial K_3}{\partial w_{jk}} &= \{f_{\theta_b}(x)\}_j \sum_i \left[\frac{\partial \Phi_{ik}}{\partial g_k} \frac{\partial g_k}{\partial w_{jk}} \log s(g_i) + \Phi_{ik} \frac{\partial \log s(g_i)}{\partial g_k} \frac{\partial g_k}{\partial w_{jk}} + \frac{\partial \Phi_{ik}}{\partial g_k} \frac{\partial g_k}{\partial w_{jk}} \right] \\
&= \{f_{\theta_b}(x)\}_j^2 \sum_i [\Phi_{kk} \Psi_{ki} \log s(g_i) + \Phi_{ik} \Psi_{ik} + \Phi_{kk} \Psi_{ki}] \\
&= \{f_{\theta_b}(x)\}_j^2 \left[\Phi_{kk} (\Psi_k \cdot \log s(g)) + (\{\Phi^\top\}_k \cdot \{\Psi^\top\}_k) + \underbrace{\Phi_{kk} (\Psi_k \cdot \mathbf{1})}_{\text{row sum is 0}} \right] \\
&= \{f_{\theta_b}(x)\}_j^2 [\Phi_{kk} (\Psi_k \cdot \log s(g)) + (\{\Phi^\top\}_k \cdot \{\Psi^\top\}_k)].
\end{aligned}$$

Thus,

$$\begin{aligned}
\text{Tr} \left(\frac{\partial K_3}{\partial w_{jk}} \right) &= \sum_{jk} [\{f_{\theta_b}(x)\}_j^2 [\Phi_{kk} (\Psi_k \cdot \log s(g)) + (\{\Phi^\top\}_k \cdot \{\Psi^\top\}_k)]] \\
&= \|f_{\theta_b}(x)\|_2^2 \cdot (\psi^\top h(x, \theta) + \mathbf{1}^\top \omega).
\end{aligned}$$

Finally, we have

$$\begin{aligned}
\text{Tr} \left(\frac{\partial^2 K}{\partial w_{jk}^2} \right) &= \text{Tr} \left[\frac{\partial K'}{\partial w_{jk}^2} + \frac{\partial K_1}{\partial w_{jk}^2} + \frac{\partial K_2}{\partial w_{jk}^2} + \frac{\partial K_3}{\partial w_{jk}^2} \right] \\
&= \|f_{\theta_b}(x')\|_2^2 \cdot \mathbf{1}^\top h(x', \theta) + G(x, x'; \theta)
\end{aligned}$$

where

$$\begin{aligned}
G(x, x'; \theta) &= -f_{\theta_b}(x')^\top f_{\theta_b}(x) \cdot \mathbf{1}^\top h(x, \theta) - f_{\theta_b}(x')^\top f_{\theta_b}(x) \cdot \mathbf{1}^\top h(x, \theta) - \|f_{\theta_b}(x)\|_2^2 \cdot \psi'^\top h(x, \theta) \\
&\quad - f_{\theta_b}^\top(x') f_{\theta_b}(x) \cdot \mathbf{1}^\top \omega' + \|f_{\theta_b}(x)\|_2^2 \cdot (\psi^\top h(x, \theta) + \mathbf{1}^\top \omega).
\end{aligned}$$

We arrive at

$$\begin{aligned}
\text{Tr} \left\{ \nabla_{\theta_t}^2 \left[\text{CE}((x, y), g_\theta) + \lambda_t \cdot \max_{\|\epsilon\|_p \leq \delta} \text{KLloss}((x, x + \epsilon), g_\theta) \right] \right\} & \quad (26) \\
&= \|f_{\theta_b}(x)\|_2^2 \cdot \mathbf{1}^\top h(x, \theta) + \lambda_t (\|f_{\theta_b}(x')\|_2^2 \cdot \mathbf{1}^\top h(x', \theta) + G(x, x'; \theta)),
\end{aligned}$$

where

$$x' = \arg \max_{\|\epsilon\|_p \leq \delta} [\text{KLloss}((x, x + \epsilon), F_\theta)] + x$$

Finally, we complete the derivation by denoting $\text{TrH}_t(x, x'; \lambda_t, \theta) \stackrel{\text{def}}{=} \text{Tr} \left\{ \nabla_{\theta_t}^2 \left[\text{CE}((x, y), g_\theta) + \lambda_t \cdot \max_{\|\epsilon\|_p \leq \delta} \text{KLloss}((x, x + \epsilon), g_\theta) \right] \right\}$.

B. Impact of Top-Layer Regularization

In this section, we provide a full description of Example 1, as well as some additional results and analysis.

- **Dataset.** We use the Two Moons Dataset where the input features $x_i \in \mathbb{R}^2$ and the label $y_i \in \{0, 1\}$ (Figure 4).
- **Network.** We use a dense network Dense(100)-ReLU-Dense(100)-ReLU-Dense(2).
- **Training without Regularization (Standard).** We train the network with AT(base), such that it is robust in an ℓ_∞ ball of size 0.02 with 1 PGD step. We use a momentum-SGD with learning rate 0.1 for 100 epochs.
- **Training with Top TrH Regularization (Top).** We further add the TrH of the top layer as a regularization term in the loss. We compute the TrH at the top layer using Proposition 1. The regularizing coefficient for the top-layer TrH is 0.5 (i.e. $loss = AT + 0.5 * \text{TrH}_{top}$) as we find it needs a stronger penalty due to the lack of TrH from other layers.

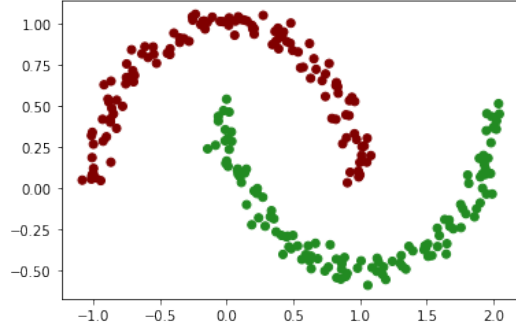


Figure 4. Visualization of Two Moons dataset. The task is to classify the points into two classes (red and green).

- **Training with Full TrH Regularization (Full).** In addition to the Standard setup, we add the TrH of the full network as a regularization term in the loss. We numerically compute the Hessian and its trace. The regularizing coefficient for the full-network TrH is 0.05 (i.e. $loss = AT + 0.05 * TrH_{full}$).

Figure 5, shows pairs of plots of **the sum and standard deviation of the eigenvalues of the Hessian matrix** across all layers, as well as for each of the three layers separately. We compare the three setting (1) no regularization (Standard, blue); (2) the top-layer TrH regularization (Top, orange); and (3) the full-network TrH regularization (Full, green).

Focusing on the top-left plot in Figure 5, we see that the TrH decreases across time with standard training (blue), but at the same time, that full-network and top-layer TrH regularization decrease it even further. In particular, top-layer TrH regularization is nearly as effective as directly regularizing the TrH for all layers. The standard deviation plots (on the right side of each TrH plot) show a decrease in the standard deviation, which implies there is a contraction effect on the eigenvalues of the Hessian, with both positive and negative values approaching towards 0. This rules out the possibility that the TrH reduction comes from an increase in the magnitude of the negative eigenvalues. In fact, TrH regularization effectively contracts the magnitude of all eigenvalues and leads to a smoother region in the loss surface.

We further plot the TrH and standard deviation of Hessian eigenvalues for each individual layer respectively (where Layer 3 is the top layer). Except for the first layer, whose eigenvalues seem to be small from the onset, the eigenvalue contraction effect is evident as training progresses, with a stronger and similar effect for both TrH regularization settings.

C. Hyper-parameters Shared by All Methods

Pre-Tuning. Training ViTs can sometimes be challenging due to a large amount of hyper-parameters. For the choice of the parameters that are shared across different defense methods, e.g. batch size, patch size, training iterations, and etc., we do a large grid search and choose the parameter setting that produce the best results on TRADES(base) and use it for all the methods. This step is referred to as pre-tuning and is done per-dataset.

Pre-selected Hyper-parameters. There is a set of hyper-parameters requiring no tuning because they are commonly selected in the literature. In the top of Table 4 and 3, we write down the these parameters and explain the reason for choosing a particular value.

Tunable Hyper-parameters. In the bottom of Table 4 and 3, we show our choice of hyper-parameters for ImageNet and CIFAR-10/100, respectively. This includes

- `optimizer`. We tested a momentum-SGD (`sgd+momentum`) and an Adam optimizer (`adam`). We found that momentum-SGD is more stable in fine-tuning the ViT from a pre-trained checkpoint.
- `base_lr`, `warm_up_iterations` and `decay_type`. We linearly increase the learning rate from 0 to the `base_lr` during `warm_up_iterations`. After warm-up, we gradually schedule the learning rate based on the `decay_type`. We experiment with a multi-step and a cosine decay and find no apparent difference between these two schedulers. In the end, we choose cosine because it has less hyper-parameters to choose compared to the multi-step one.

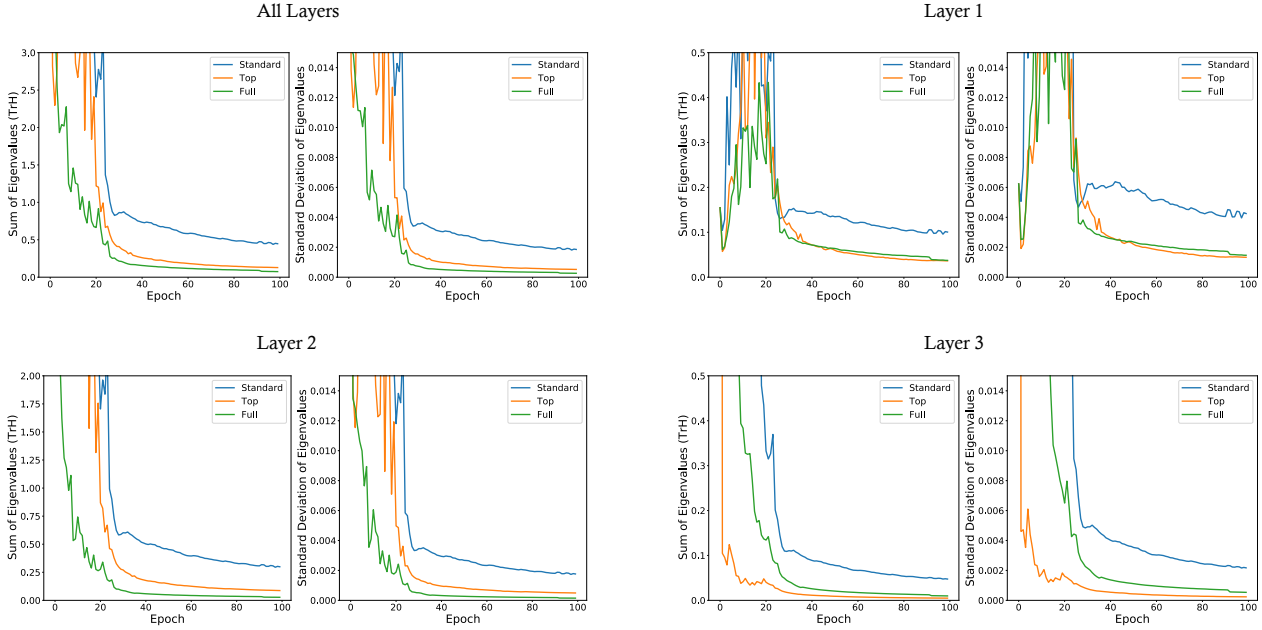


Figure 5. The figure shows pairs of plots for the sum and the standard deviation of the Hessian matrix eigenvalues. The top-left pair corresponds to the Hessian of all layers, while the rest to each of the three layers separately, with Layer 3 being the top layer (note that the sum of eigenvalues is exactly the trace of Hessian). As can be seen on the top-left, the sum and standard deviation decrease in standard training (blue) and moreover, this effect is amplified by direct TrH regularization with similar results for full network regularization (green) and top-layer regularization (orange). This similarity can be explained by our Thm.4

Pre-Selected Hyper-parameters (CIFAR-10/100)

Parameter	Reason To Select	Final Frozen Value
img_size	to be compatible with ϵ	32×32
patch_size	same as [34]	4×4
parameter_init	publicly available	ImageNet21K checkpoint
batch_size	memory	768
warm_up iterations	standard	500

Pre-tuning Stage

Parameter	Range	Explanation	Final Frozen Value
optimizer	{‘sgd+momentum’, ‘adam’}	optimizer	sgd+momentum
base_lr	{0.001, 0.01, 0.1}	initial learning rate	0.1
l2_reg	{0, 0.0001, 0.001}	coefficient for L2 regularization	0
data_aug	{‘fb’, ‘crop’}	data augmentation method	‘fb’
		‘fb’: flip and random brightness	
		‘crop’: randomly crop and upsample	
downsample	{‘cubic’, ‘nearest’, ‘bilinear’}	downsample method for the first kernel to fit the patch size from 16×16 to 4×4 [34]	cubic
patch_stride	{2, 4}	the stride to create image patches	2
data_range	{[-1, 1], [0, 1], ‘centered’}	data range	centered
		‘centered’: 0-mean and 1-std	
use_cutmix	{True, False}	whether to use cutmix augmentation	False

Table 3. Frozen Hyper-parameters for CIFAR-10 and CIFAR-100 (including DDPM images) in All Experiments.

Pre-Selected Hyper-parameters (ImageNet)

Parameter	Reason To Select	Final Frozen Value
<code>data_range</code>	to align with ImageNet21K checkpoint	$[-1, 1]$
<code>img_size</code>	to be compatible with ϵ	224×224
<code>patch_size</code>	standard	16×16
<code>parameter_init</code>	publicly available	ImageNet21K checkpoint
<code>batch_size</code>	memory	64
<code>warm_up iterations</code>	standard	500

Pre-tuning Stage			
Parameter	Range	Explanation	Final Frozen Value
<code>optimizer</code>	{'sgd+momentum', 'adam'}	optimizer	'sgd+momentum'
<code>base_lr</code>	{0.001, 0.01, 0.1}	initial learning rate	0.01
<code>decay_type</code>	{'multistep', 'cosine'}	the function used to schedule lr decay	cosine
<code>l2_reg</code>	{0.0001, 0.001}	coefficient for ℓ_2 regularization	0.0001
<code>data_aug</code>	{'fb', 'crop'}	data augmentation method	'fb'
		'fb': flip and random brightness	
		'crop': randomly crop and upsample	
<code>use_cutmix</code>	{True, False}	whether to use cutmix augmentation	False

Table 4. Frozen Hyper-parameters for ViT-B16 and ViT-L16 to reproduce results in Table. 1.

- `l2_reg`. On ImageNet, we find ℓ_2 regularization with a penalty of 0.0001 helps the baseline TRADES(base). On CIFAR-10/100, we find that ℓ_2 regularization may not be necessary when using DDPM data.
- `cutmix`. In both cases we do not find the cut mix augmentation [52] help to improve the results.
- `data_range`. On CIFAR10/100, we find that centered data, i.e. normalizing the data to have 0 mean and (close to) 1 standard deviation, provides better results than scaling the images to $[-1, 1]$ (the range of data used by the pre-trained checkpoint). We simply subtract the CIFAR images from the average of per-channel mean (0.47) and divide it with the average of per-channel standard deviation (0.25). For ImageNet, we still use $[-1, 1]$ as the data range. Notice that ϵ ball needs to be re-scaled for both data ranges describe above. For example, when reporting results on $\epsilon = 0.031$ and using centered data, we need to use $\epsilon/0.25$ as the actual noise bound passed to the attacker. When normalizing the data to $[-1, 1]$, we need to pass $\epsilon/0.5$ to the attacker.
- `patch_size`. The size of the image patch of the input sequence to ViT. 16×16 is the standard size of pre-trained ViT models on ImageNet21K. Thus, when fine-tuning on ImageNet, we use 16×16 . CIFAR images are a lot smaller compared to ImageNet images. As a result, we use a smaller patch size of 4×4 to produce more patches. Using a smaller patch size requires some modifications to ViT architecture and we discuss this in detail in Appendix F.
- `downsample` and `patch_stride`. These are particular to CIFAR images. Please refer to Appendix F for detail.

D. Hyper-parameters for Specific Methods

We fine-tune ViTs after common hyper-parameters are locked after pre-tuning. For all methods, we take 10 PGD steps on CIFAR-10/100 and 7 steps for ImageNet during the training. We report the best results for each method after trying different sets of hyper-parameters. This usually involves method-specific parameters. We elaborate what hyper-parameter is tuned as follows and report the final values used in the experiments in Table 5 (CIFAR-10/100) and 6 (ImageNet).

- **base**: we use $\lambda_t = 6$ for TRADES training and λ_t is consistent across all experiments.
- **SWA**: we use $\alpha = 0.995$ so that $\theta_{\text{avg}} \leftarrow 0.995 * \theta_{\text{avg}} + 0.005 * \theta^{(t+1)}$ as this value is used in the literature [22]. Therefore, there is no tuning in SWA.
- **S2O**: The only parameter that requires tuning is the penalty α of the second-order statistic in Eq 2. In the authors' implementation, we find $1 - \alpha$ is used to balance the regularization with the robust loss (AT or TRADES). These hyper-

parameters are hard-coded in the latest commit f2d037b¹ so we directly use their choice of hyper-parameters. Namely, for AT loss, the finally loss in S2O training is set to

$$0.9 * AT_Loss + 0.1 * S2O_Loss$$

and for TRADES training the final loss is

$$0.7 * \frac{1}{m} \sum_i^m CE((x_i, y_i), F_\theta) + 0.3 * S2O_Loss + \frac{\lambda_t}{m} \sum_i^m \max_{\|\epsilon_i\|_p \leq \delta} \text{KLloss}((x_i, \epsilon_i), F_\theta).$$

- **AWP:** The two hyper-parameters in AWP that requires tuning are ψ and δ_{awp} , where ψ is the function to measure the noise added to the weights and δ_{awp} is the noise budget. We follow the choice made by Wu et al. [50] to choose ψ as the layer-wise ℓ_2 norm function so that the noise added to the weights in each layer should no greater than the ℓ_2 norm of the weights multiplied by δ_{awp} . Namely, suppose that $\xi^{(i)}$ is the noise added to a weight matrix $W^{(i)}$ at layer i , then we project $\xi^{(i)}$ such that

$$\frac{\|\xi^{(i)} + W^{(i)}\|_2}{\|W^{(i)}\|_2} \leq \delta_{awp}.$$

For the choice of δ_{awp} , we sweep δ_{awp} over the interval $\{0.0001, 0.0005, 0.001, 0.005, 0.01\}$.

- **TrH:** The two hyper-parameters in TrH that requires tuning are the ℓ_2 weight penalty γ and the TrH penalty λ . For γ , we find 0.001 as a reasonable choice for CIFAR-10/100 and 0.0001 as a reasonable choice for ImageNet. For λ , we sweep the interval $\{0.00001, 0.00005, 0.0001, 0.0005, 0.001, 0.005, 0.01\}$. Furthermore, we also consider three types of schedulers: ‘constant’, ‘linear’, ‘multistep(0.1-0.5:0.1)’ for λ scheduling. Intuitively, a strong TrH regularization at the very beginning may lead the model to a flat highland instead of a flat minimum where we get a degenerated model. Ramping up λ to the chosen value allows the model to focus more on accuracy and robustness at the early stage. In practice, we find that CIFAR10/100 is not sensitive to the choice of the λ schedulers; however, ImageNet favors ‘linear’ or ‘multistep’ schedulers over the ‘constant’ λ .
 - ‘constant’. No λ scheduling.
 - ‘linear’. We ramp up λ from 0 to the chosen value from iteration 1 to the end.
 - ‘multistep(0.1-0.5:0.1)’. We use $0.01 * \lambda$ before finishing 10% of the total iterations. We use $0.1 * \lambda$ after finishing 10% and before 50% of the total iterations. After finishing 50% of iterations, we use λ .

E. Additional Results

Due to space limitation, we include the results on CIFAR-10/100 with ViT-B16 in Table 7 and ImageNet with Hybrid-L16 in Table 8 of the appendix. These additional results are consistent with what we have found in Section 4.2 of the paper: in CIFAR-10/100, TrH is consistently among the top or silver results; in ImageNet, TrH has significantly advantages over the other baseline methods.

F. ViT Architecture

We describe the architectures of Vision Transformers used in our experiments in Section 4.

- ViT-B16 includes 12 transformer layers with hidden size 768, MLP layer size 3072 and 12 heads in the multi-head attention.
- ViT-L16 includes 24 transformer layers with hidden size 1024, MLP layer size 4096 and 16 heads in the multi-head attention.
- Hybrid-L16 is a hybrid model of a ResNet-50 and a ViT-L16 model. The patches fed into ViT are feature representations encoded by a ResNet-50 and projected to the Transformer dimensions [15]. Dissimilar to a standard ResNet-50 feature encoder, Dosovitskiy et al. [15] replaced Batch Normalization with Group Normalization [51] and use standardized Convolution [38]. Moreover, Dosovitskiy et al. [15] removed stage 4, placed the same number of layers in stage 3 (keeping the total number of layers), and took the output of this extended stage 3 as the input of ViT.

¹<https://github.com/Alexkael/S2O/tree/f2d037b9611f7322783411825099251f7978f54e>

Fine-tuning Hyper-parameters (CIFAR-10/100, ViT-L16)

Defense	Hyper-parameter	Range	Final Choice (CIFAR-10)	Final Choice (CIFAR-100)
AT(AWP)	δ_{awp}	{0.0001, 0.0005, 0.001, 0.005, 0.01}	0.0005	0.0005
AT(SWA)	α	-	0.995	0.995
AT(S2O)	α	-	0.1	0.1
AT(TrH)	λ	{0.00001, 0.00005, 0.0001, 0.0005, 0.001, 0.005, 0.01}	0.00001	0.01
	λ schedule	{‘constant’, ‘linear’, ‘multistep’}	‘multistep’	‘multistep’
	γ	-	0.001	0.001
TRADES(AWP), $\lambda_t=6$	δ_{awp}	{0.0001, 0.0005, 0.001, 0.005, 0.01}	0.0005	0.0001
TRADES(SWA), $\lambda_t=6$	α	-	0.995	0.995
TRADES(S2O), $\lambda_t=6$	α	-	0.3	0.3
TRADES(TrH), $\lambda_t=6$	λ	{0.00001, 0.00005, 0.0001, 0.0005, 0.001, 0.005, 0.01}	0.0001	0.0001
	λ schedule	{‘constant’, ‘linear’, ‘multistep’}	‘multistep’	‘constant’
	γ	-	0.001	0.001

Fine-tuning Hyper-parameters (CIFAR-10/100, Hybrid-L16)

Defense	Hyper-parameter	Range	Final Choice (CIFAR-10)	Final Choice (CIFAR-100)
AT(AWP)	δ_{awp}	{0.0001, 0.0005, 0.001, 0.005, 0.01}	0.0005	0.0005
AT(SWA)	α	-	0.995	0.995
AT(S2O)	α	-	0.1	0.1
AT(TrH)	λ	{0.00001, 0.00005, 0.0001, 0.0005, 0.001, 0.005, 0.01}	0.0005	0.0005
	λ schedule	{‘constant’, ‘linear’, ‘multistep’}	‘multistep’	‘multistep’
	γ	-	0.001	0.001
TRADES(AWP), $\lambda_t=6$	δ_{awp}	{0.0001, 0.0005, 0.001, 0.005, 0.01}	0.0005	0.0005
TRADES(SWA), $\lambda_t=6$	α	-	0.995	0.995
TRADES(S2O), $\lambda_t=6$	α	-	0.3	0.3
TRADES(TrH), $\lambda_t=6$	λ	{0.00001, 0.00005, 0.0001, 0.0005, 0.001, 0.005, 0.01}	0.0001	0.0001
	λ schedule	{‘constant’, ‘linear’, ‘multistep’}	‘multistep’	‘multistep’
	γ	-	0.001	0.001

Table 5. Hyper-parameters used in each defense and the values used to reproduce CIFAR10/100 results in Table. 1.

The pretrained ViT-B16 and ViT-L16 checkpoints use patch size 16×16 . However, since the images in CIFAR10/100 are of size 32×32 , there will be only 4 patches when using the original patch size. Therefore, we downsample the kernel of the first convolution to produce image patches of 4×4 . Among different ways of downsampling we find the cubic interpolation gives the best results, which is the one chosen in pre-tuning as discussed in Appendix C. Indeed, Mahmood et al. [34] empirically finds that such down-sampling provides better results for CIFAR10 images. Furthermore, in generating patches, we also use a stride of 2 instead of 4, because we find using overlapped patches increases the sequence length and results in better performance.

G. TrH Regularization for Other Adversarial Losses

In this section, we apply TrH regularization to some additional robust losses other than AT or TRADES.

G.1. ALP [30]

Similar to TRADES, Adversarial Logit Pairing (ALP) [30] is another method that pushes points away from the decision boundary by regularizing the ℓ_2 difference between the clean and the adversarial softmax outputs. Formally, ALP minimizes

Fine-tuning Hyper-parameters (ImageNet, ViT-B16)

Defense	Hyper-parameter	Range	Final Choice (ℓ_∞)	Final Choice (ℓ_2)
AT(AWP)	δ_{awp}	{0.0001, 0.0005, 0.001, 0.005, 0.01}	0.0001	0.0001
AT(SWA)	α	-	0.995	0.995
AT(S2O)	α	-	0.1	0.1
AT(TrH)	λ	{0.00001, 0.00005, 0.0001, 0.0005, 0.001, 0.005, 0.01}	0.0001	0.00005
	λ schedule	{‘constant’, ‘linear’, ‘multistep’}	‘multistep’	‘linear’
	γ	-	0.0001	0.0001
TRADES(AWP), $\lambda_t=6$	δ_{awp}	{0.0001, 0.0005, 0.001, 0.005, 0.01}	0.0001	0.0001
TRADES(SWA), $\lambda_t=6$	α	-	0.995	0.995
TRADES(S2O), $\lambda_t=6$	α	-	0.3	0.3
TRADES(TrH), $\lambda_t=6$	λ	{0.00001, 0.00005, 0.0001, 0.0005, 0.001, 0.005, 0.01}	0.00005	0.00005
	λ schedule	{‘constant’, ‘linear’, ‘multistep’}	‘linear’	‘linear’
	γ	-	0.0001	0.0001

Fine-tuning Hyper-parameters (ImageNet, ViT-L16)

Defense	Hyper-parameter	Range	Final Choice (ℓ_∞)	Final Choice (ℓ_2)
AT(AWP)	δ_{awp}	{0.0001, 0.0005, 0.001, 0.005, 0.01}	0.0001	0.0001
AT(SWA)	α	-	0.995	0.995
AT(S2O)	α	-	0.1	0.1
AT(TrH)	λ	{0.00001, 0.00005, 0.0001, 0.0005, 0.001, 0.005, 0.01}	0.0005	0.0005
	λ schedule	{‘constant’, ‘linear’, ‘multistep’}	‘multistep’	‘linear’
	γ	-	0.0001	0.0001
TRADES(AWP), $\lambda_t=6$	δ_{awp}	{0.0001, 0.0005, 0.001, 0.005, 0.01}	0.0001	0.0001
TRADES(SWA), $\lambda_t=6$	α	-	0.995	0.995
TRADES(S2O), $\lambda_t=6$	α	-	0.3	0.3
TRADES(TrH), $\lambda_t=6$	λ	{0.00001, 0.00005, 0.0001, 0.0005, 0.001, 0.005, 0.01}	0.0005	0.00005
	λ schedule	{‘constant’, ‘linear’, ‘multistep’}	‘multistep’	‘multistep’
	γ	-	0.0001	0.0001

Table 6. Hyper-parameters used in each defense and the values used to reproduce ImageNet results in Table. 1.

$\ell_\infty(\delta = 8/255)$ SE= $\pm 0.5\%$	ViT-B16			
	CIFAR-10		CIFAR-100	
	Clean(%)	AA(%)	Clean (%)	AA(%)
AT(base)	87.5	60.3	60.0	30.4
AT(SWA)	86.9	60.4	64.1	33.7
AT(S2O)	86.8	60.4	63.2	31.5
AT(AWP)	87.3	<u>61.3</u>	61.5	32.2
AT(TrH)	88.4	61.5	65.0	<u>33.0</u>
TRADES(base)	85.4	<u>60.8</u>	58.6	30.5
TRADES(SWA)	85.6	<u>60.6</u>	62.7	33.0
TRADES(S2O)	85.9	61.1	63.5	31.5
TRADES(AWP)	84.7	<u>60.1</u>	60.8	<u>32.2</u>
TRADES(TrH)	85.8	61.1	63.8	33.0

Table 7. Additional results for CIFAR-10/100 using ViT-B16. Clean: % of Top-1 correct predictions. AA: % of Top-1 correct predictions under AutoAttack. A max Standard Error (SE) [45] = $\sqrt{0.5 * (1 - 0.5) / m}$ (m as the number of test examples) is computed for each dataset. The best results appear in bold. Underlined results are those that fall within the SE range of the result and are regarded roughly equal to the best result.

ImageNet SE= $\pm 0.2\%$ Defense	Hybrid-L16			
	$\ell_\infty(\delta = 4/255)$		$\ell_2(\delta = 3.0)$	
	Clean(%)	AA(%)	Clean(%)	AA(%)
AT(base)	72.6	40.7	72.2	40.6
AT(SWA)	72.7	40.4	72.7	40.5
AT(S2O)	72.8	43.6	72.3	40.9
AT(AWP)	67.7	39.4	67.9	40.3
AT(TrH)	75.0	46.2	74.4	45.9
TRADES(base)	79.5	37.6	78.0	38.6
TRADES(SWA)	72.9	40.9	71.3	40.8
TRADES(S2O)	73.8	41.3	72.2	41.2
TRADES(AWP)	66.4	38.8	65.3	40.9
TRADES(TrH)	75.9	45.7	73.3	45.6

Table 8. Additional Results for ImageNet using Hybrid-L16. Clean: % of Top-1 correct predictions. AA: % of Top-1 correct predictions under AutoAttack. A max Standard Error (SE) [45] = $\sqrt{0.5 * (1 - 0.5) / m}$ (m as the number of test examples) is computed for each dataset. The best results appear in bold. Underlined results are those that fall within the SE range of the result and are regarded roughly equal to the best result.

the following loss during training,

$$\hat{R}_A(\theta, D^m) \stackrel{\text{def}}{=} \frac{1}{m} \sum_{(x,y) \in D^m} \text{CE}((x', y), g_\theta) + \lambda_A \|s(g_\theta(x)) - s(g_\theta(x'))\|_2^2$$

where $x' = x + \arg \max_{\|\epsilon\|_p \leq \delta} \text{CE}((x + \epsilon, y), g_\theta)$.

We hereby derive TrH regularization for $\hat{R}_A(\theta, D^m)$. Using Proposition 1, we know that

$$\text{TrH}(\text{CE}((x', y), g_\theta)) = \|f_{\theta_b}(x')\|_2^2 \cdot \mathbf{1}^\top h(x', \theta).$$

The rest of this section will focus on the ℓ_2 distance loss,

$$S \stackrel{\text{def}}{=} \|s(g_\theta(x)) - s(g_\theta(x'))\|_2^2 = \sum_i (s(g_i) - s(g'_i))^2, \quad (27)$$

where $g = g_\theta(x), g' = g_\theta(x')$. To compute $\text{Tr}(\nabla_{\theta_t}^2 S)$, we need to re-use Lemma 1 and 2 to obtain the derivatives of the softmax and log-softmax outputs, i.e.

$$\frac{\partial s(g_\theta(x))}{g_\theta(x)} = \Phi \stackrel{\text{def}}{=} \text{diag}(s(g_\theta(x))) - s(g_\theta(x)) \cdot s(g_\theta(x))^\top$$

and $\frac{\partial \log s(g_\theta(x))}{g_\theta(x)} = \Psi \stackrel{\text{def}}{=} I - \mathbf{1} \cdot s(g_\theta(x))^\top,$

as well as

$$\frac{\partial \Phi_{ik}}{\partial \{g_\theta(x)\}_k} = \Phi_{kk} \Psi_{ki}.$$

For the ease of notation, we let $w \stackrel{\text{def}}{=} \theta_t$ be the weights of the top-layer. Now we are ready to write the first-order derivative of S w.r.t w_{jk} as follows

$$\begin{aligned} \frac{\partial S}{\partial w_{jk}} &= \sum_i 2(s(g_i) - s(g'_i)) \left[\frac{\partial s(g_i)}{\partial w_{jk}} - \frac{\partial s(g'_i)}{\partial w_{jk}} \right] \\ &= 2 \sum_i (s(g_i) - s(g'_i)) (\Phi_{ik} \{f_{\theta_b}(x)\}_j - \Phi'_{ik} \{f_{\theta_b}(x')\}_j). \end{aligned}$$

The second-order derivative is equal to

$$\begin{aligned}\frac{\partial^2 S}{\partial w_{jk}^2} &= 2 \sum_i \left[\frac{\partial s(g_i)}{\partial w_{jk}} - \frac{\partial s(g'_i)}{\partial w_{jk}} \right] (\Phi_{ik} \{f_{\theta_b}(x)\}_j - \Phi'_{ik} \{f_{\theta_b}(x')\}_j) + (s(g_i) - s(g'_i)) \left[\frac{\partial \Phi_{ik}}{\partial w_{jk}} \{f_{\theta_b}(x)\}_j - \frac{\partial \Phi'_{ik}}{\partial w_{jk}} \{f_{\theta_b}(x')\}_j \right] \\ &= 2 \sum_i (\Phi_{ik} \{f_{\theta_b}(x)\}_j - \Phi'_{ik} \{f_{\theta_b}(x')\}_j)^2 + (s(g_i) - s(g'_i)) (\Phi_{kk} \Psi_{ki} \{f_{\theta_b}(x)\}_j^2 - \Phi'_{kk} \Psi'_{ki} \{f_{\theta_b}(x')\}_j^2).\end{aligned}\quad (28)$$

Similar to TRADES, if one stops gradients over the clean logit g , then Eq. 28 can be simplified as,

$$\begin{aligned}\frac{\partial^2 S}{\partial w_{jk}^2} &= 2 \sum_i (\Phi'_{ik} \{f_{\theta_b}(x')\}_j)^2 + (s(g_i) - s(g'_i)) (-\Phi'_{kk} \Psi'_{ki} \{f_{\theta_b}(x')\}_j^2) \\ &= 2 \{f_{\theta_b}(x')\}_j^2 \left(\|\Phi_k\|_2^2 - \Phi'_{kk} ((s(g) - s(g'))^\top \Psi'_k) \right).\end{aligned}$$

Therefore, the trace of Hessian is equal to,

$$\begin{aligned}\text{Tr}(\nabla_{\theta_t}^2 S) &= \sum_{jk} 2 \{f_{\theta_b}(x')\}_j^2 \left(\|\Phi_k\|_2^2 - \Phi'_{kk} ((s(g) - s(g'))^\top \Psi'_k) \right) \\ &= 2 \|f_{\theta_b}(x')\|_2^2 \cdot \sum_k \left(\|\Phi_k\|_2^2 - \Phi'_{kk} ((s(g) - s(g'))^\top \Psi'_k) \right).\end{aligned}$$

If the gradient over g is kept, then one can sum over the feature dimension j and the class dimension k in Eq. 28. To put together, the TrH regularization term for ALP is given as follows:

$$\frac{1}{m} \sum_{(x,y) \in D^m} \|f_{\theta_b}(x')\|_2^2 \cdot \mathbf{1}^\top h(x', \theta) + \lambda_A \cdot \text{Tr}(\nabla_{\theta_t}^2 S).$$

G.2. MART [47]

In [47], Wang et al. proposed MART as a robust training loss that focus more on points that are not classified correctly. Different from AT, TRADES and ALP, MART explicitly aims to increase the margin between the top prediction and the second best candidate. In what follows we provide the TrH regularization for MART. We denote the MART loss as \hat{R}_M , which contains two components: a boosted Cross-Entropy (BCE) loss and a weighted KL-Divergence (WKL),

$$\hat{R}_M(\theta, D^m) \stackrel{\text{def}}{=} \frac{1}{m} \sum_{(x,y) \in D^m} \text{BCE}((x', y), g_\theta) + \lambda_m \text{WKL}((x, x'), g_\theta),$$

where

$$\text{BCE}((x', y), g_\theta) \stackrel{\text{def}}{=} \text{CE}((x, y), g_\theta) + (-\log(1 - \max_{\kappa \neq y} s(\{g_\theta(x')\}_\kappa))),$$

$$\text{and, } \text{WKL}((x, x'), g_\theta) \stackrel{\text{def}}{=} \text{KL}(s(g_\theta(x)) \| s(g_\theta(x')))(1 - s(\{g_\theta(x)\}_y)).$$

Here

$$x' = x + \arg \max_{\|\epsilon\|_p \leq \delta} \text{CE}((x, y), \theta). \quad (29)$$

First, we derive TrH of the BCE loss with respect to the top-layer weights θ_t ,

$$\text{Tr}(\nabla_{\theta_t}^2 \text{BCE}) = \text{Tr}(\nabla_{\theta_t}^2 [\text{CE}((x, y), g_\theta)]) + \text{Tr}(\nabla_{\theta_t}^2 [-\log(1 - \max_{\kappa \neq y} s(\{g_\theta(x')\}_\kappa))]).$$

Using intermediate steps from the proof of Proposition 2 in Appendix A, we have that

$$\text{Tr}(\nabla_{\theta_t}^2 [\text{CE}((x, y), g_\theta)]) = \|f_{\theta_b}(x)\|_2^2 \cdot \mathbf{1}^\top h(x, \theta).$$

In order to compute $\text{Tr}(\nabla_{\theta_t}^2 [-\log(1 - \max_{\kappa \neq y} s(\{g_\theta(x')\}_\kappa)])$, we make use of Lemma 1 and 2 to obtain the derivatives of the softmax and log-softmax outputs,

$$\frac{\partial s(g_\theta(x'))}{g_\theta(x')} = \Phi' \stackrel{\text{def}}{=} \text{diag}(s(g_\theta(x'))) - s(g_\theta(x')) \cdot s(g_\theta(x'))^\top$$

and $\frac{\partial \log s(g_\theta(x'))}{g_\theta(x')} = \Psi' \stackrel{\text{def}}{=} I - \mathbf{1} \cdot s(g_\theta(x'))^\top,$

as well as,

$$\frac{\partial \Phi'_{ik}}{\partial \{g_\theta(x')\}_k} = \Phi'_{ik} \Psi'_{ki}.$$

Let us denote $K = -\log(1 - \max_{\kappa \neq y} s(\{g_\theta(x')\}_\kappa))$ and $w = \theta_t$ for the ease of notation. Then the first-order derivative of K w.r.t. w_{jk} is,

$$\frac{\partial K}{\partial w_{jk}} = \frac{\Phi'_{\kappa^*k}}{1 - s(\{g_\theta(x')\}_{\kappa^*})} \{f_{\theta_b}(x')\}_j,$$

where

$$\kappa^* = \arg \max_{\kappa \neq y} s(\{g_\theta(x')\}_\kappa).$$

The second-order derivative is,

$$\begin{aligned} \frac{\partial^2 K}{\partial w_{jk}^2} &= \frac{\frac{\partial \Phi'_{\kappa^*k}}{\partial w_{jk}} (1 - s(\{g_\theta(x')\}_{\kappa^*})) + \Phi'_{\kappa^*k} \Phi'_{\kappa^*k} \{f_{\theta_b}(x')\}_j}{(1 - s(\{g_\theta(x')\}_{\kappa^*}))^2} \{f_{\theta_b}(x')\}_k \\ &= \frac{\Phi'_{kk} \Psi'_{k\kappa^*} \{f_{\theta_b}(x')\}_k (1 - s(\{g_\theta(x')\}_{\kappa^*})) + \Phi'_{\kappa^*k} \Phi'_{\kappa^*k} \{f_{\theta_b}(x')\}_j}{(1 - s(\{g_\theta(x')\}_{\kappa^*}))^2} \{f_{\theta_b}(x')\}_j \\ &= \{f_{\theta_b}(x')\}_j^2 \left[\frac{\Phi'_{\kappa^*k} \Phi'_{\kappa^*k}}{1 - s(\{g_\theta(x')\}_{\kappa^*})} + \frac{\Phi_{\kappa^*k}^{\prime 2}}{(1 - s(\{g_\theta(x')\}_{\kappa^*}))^2} \right]. \end{aligned}$$

Thus,

$$\begin{aligned} \text{Tr}\left(\frac{\partial^2 K}{\partial w_{jk}^2}\right) &= \sum_{jk} \{f_{\theta_b}(x')\}_j^2 \left[\frac{\Phi'_{\kappa^*k} \Phi'_{\kappa^*k}}{1 - s(\{g_\theta(x')\}_{\kappa^*})} + \frac{\Phi_{\kappa^*k}^{\prime 2}}{(1 - s(\{g_\theta(x')\}_{\kappa^*}))^2} \right] \\ &= \|f_{\theta_b}(x')\|_2^2 \sum_k \left[\frac{\Phi'_{\kappa^*k} \Phi'_{\kappa^*k}}{1 - s(\{g_\theta(x')\}_{\kappa^*})} + \frac{\Phi_{\kappa^*k}^{\prime 2}}{(1 - s(\{g_\theta(x')\}_{\kappa^*}))^2} \right], \end{aligned}$$

and

$$\text{Tr}(\nabla_{\theta_t}^2 \text{BCE}) = \|f_{\theta_b}(x)\|_2^2 \cdot \mathbf{1}^\top h(x, \theta) + \|f_{\theta_b}(x')\|_2^2 \sum_k \left[\frac{\Phi'_{\kappa^*k} \Phi'_{\kappa^*k}}{1 - s(\{g_\theta(x')\}_{\kappa^*})} + \frac{\Phi_{\kappa^*k}^{\prime 2}}{(1 - s(\{g_\theta(x')\}_{\kappa^*}))^2} \right].$$

Next, we derive the trace of Hessian for WKL loss. Similarly to before, by stopping the gradient over the clean logit $g_\theta(x)$, the trace of Hessian of WKL will be the same as the KL loss used in TRADES, which has been shown in Proposition 2. Namely, in this case

$$\text{Tr}(\nabla_{\theta_t}^2 \text{WKL}) = \|f_{\theta_b}(x')\|_2^2 \cdot \mathbf{1}^\top h(x', \theta).$$

On the other hand, if the gradient on $g_\theta(x)$ is computed, there is an additional term in $\text{Tr}(\nabla_{\theta_t}^2 \text{WKL})$ (similar but more complicated than $G(x, x'; \theta)$ derived in the proof of Proposition 2 in Appendix A), which we will leave as future work. Finally, we present the TrH regularization for MART as follows,

$$\text{TrH}_M(x, x'; \lambda_m, \theta) = \text{Tr}(\nabla_{\theta_t}^2 \text{BCE}) + \lambda_m \text{Tr}(\nabla_{\theta_t}^2 \text{WKL}).$$

This concludes our derivations of the TrH regularization for the MART loss.